

1 Anti-clustering in the national SARS-CoV-2 2 daily infection counts

3 Boudewijn F. Roukema^{1,2}

4 ¹Institute of Astronomy, Faculty of Physics, Astronomy and Informatics, Nicolaus
5 Copernicus University, Grudziadzka 5, 87-100 Toruń, Poland

6 ²Univ Lyon, Ens de Lyon, Univ Lyon1, CNRS, Centre de Recherche Astrophysique de
7 Lyon UMR5574, F-69007, Lyon, France

8 Corresponding author:

9 Boudewijn F. Roukema¹

10 Email address: boud@astro.uni.torun.pl

11 ABSTRACT

12 The noise in daily infection counts of an epidemic should be super-Poissonian due to intrinsic epidemiological and administrative clustering. Here, we use this clustering to classify the official national SARS-CoV-2 daily infection counts and check for infection counts that are unusually anti-clustered. We adopt a one-parameter model of ϕ_i' infections per cluster, dividing any daily count n_i into n_i/ϕ_i' 'clusters', for 'country' i . We assume that n_i/ϕ_i' on a given day j is drawn from a Poisson distribution whose mean is robustly estimated from the 4 neighbouring days, and calculate the inferred Poisson probability P'_{ij} of the observation. The P'_{ij} values should be uniformly distributed. We find the value ϕ_i that minimises the Kolmogorov–Smirnov distance from a uniform distribution. We investigate the (ϕ_i, N_i) distribution, for total infection count N_i . We consider consecutive count sequences above a threshold of 50 daily infections. We find that most of the daily infection count sequences are inconsistent with a Poissonian model. Most are found to be consistent with the ϕ_i model, with the 28-, 14- and 7-day least noisy sequences for several countries being best modelled as sub-Poissonian, suggesting a distinct epidemiological family. The 28-day least noisy sequence of Algeria has a preferred model that is strongly sub-Poissonian, with $\phi_i^{28} < 0.1$. Tajikistan, Turkey, Russia, Belarus, Albania, United Arab Emirates, and Nicaragua have preferred models that are also sub-Poissonian, with $\phi_i^{28} < 0.5$. A statistically significant ($P^\tau < 0.05$) correlation was found between the lack of media freedom in a country, as represented by a high *Reporters sans frontières* Press Freedom Index (PFI²⁰²⁰), and the lack of statistical noise in the country's daily counts. The ϕ_i model appears to be an effective detector of suspiciously low statistical noise in the national SARS-CoV-2 daily infection counts.

31 1 INTRODUCTION

32 The daily counts of new, laboratory-confirmed infections with severe acute respiratory syndrome coronavirus 2 (SARS-CoV-2) constitute one of the key statistics followed by citizens and health agencies around the world in the ongoing 2019–2020 coronavirus disease 2019 (COVID-19) pandemic (Huang et al. 2020b; Li et al. 2020). Can these counts be classified in a way that makes as few epidemiological assumptions as possible, as motivation for deeper analysis to either validate or invalidate the counts? While full epidemiological modelling and prediction is a vital component of COVID-19 research (Chowdhury et al. 2020; Kim et al. 2020; Molina-Cuevas 2020; Jiang, Zhao & Shao 2020; Afshordi et al. 2020), these cannot be accurately used to study the pandemic as a whole – a global phenomenon by definition – if the data at the global level is itself inaccurate. Knowledge of the global state of the current pandemic is weakened if any of the national-level SARS-CoV-2 infection data have been artificially interfered with by the health agencies providing that data or by other actors involved in the chain of data lineage (Thomas et al., 2017). Since personal medical data are private information, only a limited number of individuals at health agencies are expected to be able to check the validity of these counts based on original records. Nevertheless, artificial interventions in the counts could potentially reveal themselves in statistical properties of the counts. Unusual statistical properties in a

47 wide variety of quantitative data sometimes appear, for example, as anomalies related to Benford’s law
48 (Newcomb 1881; Nigrini & Miller 2009), as in the 2009 first round of the Iranian presidential election
49 (Roukema, 2014, 2015; Mebane, 2010). Benford’s law analysis has been used to argue that countries with
50 higher democracy indices, high gross domestic product, and better health system indices tend to have
51 a lower probability of having manipulated their key COVID-19 related cumulative counts (confirmed
52 cases and deaths, Balashov, Yan & Zhu 2020). For other Benford’s law COVID-19 count analyses, see
53 Koch & Okamura (2020) and Lee et al. (2020). For the politics of organisational strategies regarding
54 open government data, see Ruijter et al. (2019).

55 Here, we check the compatibility of noise in the official national SARS-CoV-2 daily infection counts,
56 $n_i(t)$, for country¹ i on date t , with expectations based on the Poisson distribution (Poisson (1837); for a
57 review, see, e.g., Johnson et al. 2005). The Poisson distribution is motivated by the one-day time scale for
58 an infection count being several times shorter than the dominant time scale involved, the incubation time
59 scale, estimated at about five days (Lauer et al., 2020; Yang et al., 2020), with a 95% confidence interval
60 (CI) from about one to 15 days (Yang et al., 2020). Since each infected person typically infects about two
61 to three others ($R_0 \sim 2.4\text{--}3.3$ at 95% (CI), Billah et al. 2020), these secondarily infected people would
62 typically be assessed as SARS-CoV-2 positive on independent days, if they were diagnosed immediately
63 after the onset of symptoms, with instantaneous laboratory testing and test results reported instantly in
64 the official national count data. In reality, delays for diagnosis, testing and reporting and collating the test
65 results are random processes which should further add delays that reduce correlations among positive
66 test results between distinct nearby days; a Poissonian process is a simple hypothesis for each of these
67 separate processes. Poisson processes are both additive and infinitely divisible (Johnson et al., 2005, §4),
68 so the combination of these processes can reasonably yield an overall Poisson process.

69 However, it is unlikely that any real count data will be fully modelled by a Poisson distribution, both
70 due to the complexity of the logical tree of time-dependent intrinsic epidemiological infection as well
71 as administrative effects in the SARS-CoV-2 testing procedures, and the sub-national and national level
72 procedures for collecting and validating data to produce a national health agency’s official report. In
73 particular, clusters of infections on a scale of ϕ_i^t infections per cluster, either intrinsic or in the testing
74 and administrative pipeline, would tend to cause relative noise to increase from a fraction of $1/\sqrt{n_i}$ for
75 pure Poisson noise up to $\sqrt{\phi_i^t/n_i}$, greater by a factor of $\sqrt{\phi_i^t}$. This overdispersion has been found, for
76 example, for SARS-CoV-2 transmission (Endo et al., 2020; He et al., 2020) and for COVID-19 death
77 rate counts in the United States (Kim et al., 2020).

78 In contrast, it is difficult to see how anti-Poissonian smoothing effects could occur, unless they were
79 imposed administratively. For example, an administrative office might impose (or have imposed on it by
80 political authorities) a constraint to validate a fixed or slowly and smoothly varying number of SARS-
81 CoV-2 test result files per day, independently of the number received or queued; this would constitute an
82 example of an artificial intervention in the counts that would weaken the epidemiological usefulness of
83 the data.

84 A one-parameter model to allow for the clustering is proposed in this paper, and used to classify the
85 counts. We allow the parameter to take on an effective anti-clustering value, in order to allow the data
86 to freely determine its optimal value, without forcing overdispersion. While a distribution of clustering
87 values for a given country is likely to be more realistic than a single value, Occam’s razor favours
88 adding as few parameters as possible. For example, a power-law distribution of arbitrary (negative)
89 index would require a second parameter to truncate the tail in non-convergent cases. While the one-
90 parameter anti-clustering value is a simplified model, it has the advantage of allowing a straightforward,
91 though simplified, interpretation in terms of clustering. If the one-parameter method proposed here is
92 found to viable, then the method could be extended by including models of directly observed estimates
93 of SARS-CoV-2 clustering.

94 As an alternative to this clustering model, we also consider a negative binomial distribution (e.g.
95 Johnson et al., 2005, §5). Lloyd-Smith et al. (2005) found the negative binomial distribution, as a mix
96 of Poisson distributions over a Gamma distribution, to be better at modelling secondary infections by
97 SARS-CoV-1 (and other infectious agents) than Poisson and geometric distributions, quantifying what
98 are referred to as ‘superspreader’ events in an epidemic. This has also been found to be relevant to SARS-

¹No position is taken in this paper regarding jurisdiction over territories; the term ‘country’ is intended here as a neutral term without supporting or opposing the formal notion of state. Apart from minor changes for technical reasons, the ‘countries’ are defined by the data sources.

99 CoV-2 secondary infections (Endo et al., 2020; He et al., 2020). However, since the negative binomial
100 model only allows overdispersion with respect to the Poisson model, it is unlikely to provide the best
101 model for data which may have been artificially modified to the extent of becoming sub-Poissonian.
102 More in-depth models of clustering, called “burstiness” in stochastic models of discrete event counts,
103 include power-law models (Barabási, 2005; Goh & Barabasi, 2006).

104 The method is presented in §2. Section §2.1 describes the choice of data set and the definition,
105 for any given country, of a consecutive time sequence that has high enough daily infection counts for
106 Poisson distribution analysis to be reasonable. The method of analysis is given in §2.3 for full sequences
107 (§2.3.1), subsequences (§2.3.2) and alternatives to the main method (§2.4). Results are presented in §3.
108 A non-parametric comparison with the *Reporters sans frontières* Press Freedom Index, which should
109 not have any relation to noise in SARS-CoV-2 daily counts in the absence of a sociological connection,
110 is provided in §3.3. Qualitative discussion of the results is given in §4. Conclusions are summarised
111 in §5. This work is intended to be fully reproducible by independent researchers using the MANEAGE
112 framework; it was produced using commit 72242ca of the live GIT repository <https://codeberg.org/boud/subpoisson> on a computer with Little Endian x86_64 architecture; the source is archived
113 at zenodo.4765705 and `sw:h:1:rev:27ac91a5b79d4dfe6d17ee2a43d3b441efdb22c7`.

115 2 METHOD

116 2.1 SARS-CoV-2 infection data

117 Two obvious choices of a dataset for national daily SARS-CoV-2 counts would be those provided by
118 the World Health Organization (WHO)² or those curated by the Wikipedia *WikiProject COVID-19 Case*
119 *Count Task Force*³ in *medical cases chart* templates (hereafter, C19CCTF). While WHO has published
120 a wide variety of documents related to the COVID-19 pandemic, it does not appear to have published
121 details of how national reports are communicated to it and collated. Given that most government agencies
122 and systems of government procedures tend to lack transparency, despite significant moves towards
123 forms of open government (Yu & Robinson, 2012) in many countries, data lineage tracing from national
124 governments to WHO is likely to be difficult in many cases. In contrast, the curation of official gov-
125 ernment SARS-CoV-2 daily counts by the Wikipedia *WikiProject COVID-19 Case Count Task Force*
126 follows a well-established technology of tracking data lineage. The Wikipedia community high-tempo
127 collaborative editing that has taken place in response to the COVID-19 pandemic is well quantified
128 (Keegan & Tan, 2020). The John Hopkins University Center for Systems Science and Engineering cu-
129 rated set of official COVID-19 data is discussed below.

130 Unfortunately, it is clear that in the WHO data, there are several cases where two days’ worth of
131 detected infections appear to be listed by WHO as a sequence of two days j and $j + 1$ on which all
132 the infections are allocated to the second of the two days, with zero infections on the first of the pair.
133 There are also some sequences in the WHO data where the day listed with zero infections is separated
134 by several days from a nearby day with double the usual amount of infections. This is very likely an
135 effect of difficulties in correctly managing world time zones, or time zone and sleep schedule effects, in
136 any of several levels of the chains of communication between health agencies and WHO. In other words,
137 there are several cases where a temporary sharp jump or drop in the counts appears in the data but is
138 reasonably interpreted as a timing artefact. Whatever the reason for the effect, this effect will tend to
139 confuse the epidemiological question of interest here: the aim is to globally characterise the noise and to
140 highlight countries where unusual smoothing may have taken place.

141 We quantify this jump/drop problem as follows. We consider a pair of days j , $j + 1$ for a given
142 country to be a jump if the absolute difference in counts, $|n_i(j + 1) - n_i(j)|$, is greater than the mean,
143 $(n_i(j + 1) + n_i(j))/2$. In the case of a pair in which one value is zero, the absolute difference is twice
144 the mean, and the condition is necessarily satisfied. We evaluate the number of jumps N_{jump} for both the
145 WHO data and the C19CCTF *medical cases chart* data, starting, for any given country, from the first day
146 with at least 50 infections. Figure 1 shows N_{jump} for the 137 countries in common to the two data sets;
147 there are 237 countries in the WHO data set and 139 in the C19CCTF data. It is clear that most countries
148 have fewer jumps or drops in the Wikipedia data set than in the WHO data set.

²[https://covid19.who.int/WHO-COVID-19-global-data.csv;\(archive\)](https://covid19.who.int/WHO-COVID-19-global-data.csv;(archive))

³https://en.wikipedia.org/w/index.php?title=Wikipedia:WikiProject_COVID-19/Case_Count_Task_Force&oldid=1001119689

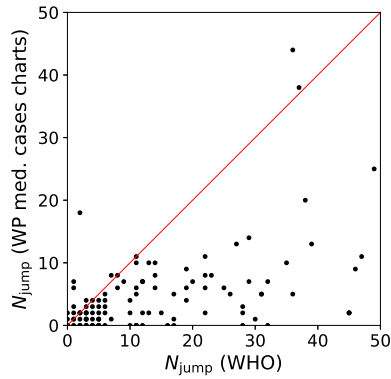


Figure 1. Number N_{jump} of sudden jumps or drops in counts on adjacent days in WHO and Wikipedia *WikiProject COVID-19 Case Count Task Force medical cases chart* national daily SARS-CoV-2 infection counts for countries present in both data sets. A line illustrates equal quality of the two data sets. The C19CCTF version of the data is clearly less affected by sudden jumps than the WHO data. Plain-text table: [zenodo.4765705/WHO_vs_WP_jumps.dat](https://zenodo.org/record/4765705/files/WHO_vs_WP_jumps.dat).

149 Thus, at least for the purposes of understanding intrinsic and administrative clustering, the
 150 C19CCTF *medical cases chart* data appear to be the better curated version of the national daily
 151 SARS-CoV-2 infection counts as reported by official agencies. The detailed download and extraction
 152 script of national daily SARS-CoV-2 infection data from these templates and the resulting data file
 153 [zenodo.4765705/WP_C19CCTF_SARSCoV2.dat](https://zenodo.org/record/4765705/files/WP_C19CCTF_SARSCoV2.dat) (downloaded 6 May 2021) are available in the reproducibility
 154 package associated with this paper (§Code availability). Dates without data are omitted; this
 155 should have an insignificant effect on the analysis if these are due to low infection counts.

156 Another global collection of daily SARS-CoV-2 counts that could be considered is the John Hopkins
 157 University Center for Systems Science and Engineering (JHU CSSE) git repository. Unfortunately, for
 158 several countries, the JHU CSSE data are provided for sub-national divisions rather than as official national
 159 statistics, making the dataset inhomogeneous for the purposes of this study. Artificial interference
 160 in the data at the national level will not be shown in data that is the sum of data obtained directly from
 161 sub-national geographical/political divisions. Moreover, detailed data provenance analysis (which exact
 162 government URL did a particular count come from? where is the archived version of the data of the
 163 original URL?) appears to be more difficult for the JHU CSSE data than for the C19CCTF data. Never-
 164 theless, for completeness, the JHU CSSE data is analysed using the same method as the main analysis,
 165 with results presented as tables in Appendix A.

166 The full set of C19CCTF data includes many days, especially for countries or territories (as defined
 167 by the data source) of low populations, with low values, including zero and one. The standard deviation
 168 of a Poisson distribution (Poisson, 1837) of expectation value N is \sqrt{N} , giving a fractional error of $1/\sqrt{N}$.
 169 Even taking into account clustering or anticlustering of data, inclusion of these periods of close to zero
 170 infection counts would contribute noise that would overwhelm the signal from the periods of higher
 171 infection rates for the same or other countries. In the time sequences of SARS-CoV-2 infection counts,
 172 chaos in the administrative reactions to the initial stages of the pandemic will tend to create extra noise,
 173 so it is reasonable to choose a moderately high threshold at which the start and end of a consecutive
 174 sequence of days should be defined for analysis. Here, we set the threshold for a sequence to start as a
 175 minimum of 50 infections in a single day. The sequence is continued for at least 7 days (if available in
 176 the data), and stops when the counts drop below the same threshold for 2 consecutive days. The cutoff
 177 criterion of 2 consecutive days avoids letting the analysable sequence be too sensitive to individual days
 178 of low fluctuations. If the resulting sequence includes less than 7 days, the sequence is rejected as having
 179 insufficient signal to be analysed.

180 2.2 RSF Press Freedom Index

181 The *Reporters sans frontières* (RSF) Press Freedom Index is derived annually from an 87-question
 182 survey translated into 20 languages and sent to ‘media professionals, lawyers and sociologists’

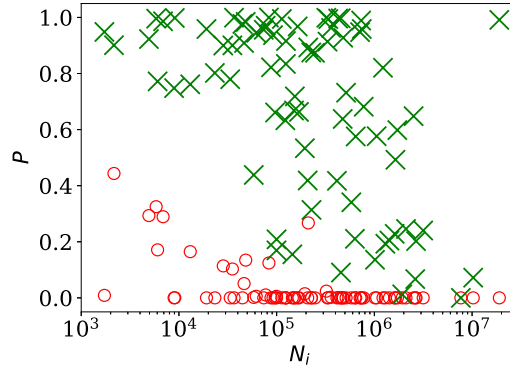


Figure 2. Probability of the noise in the country-level daily SARS-CoV-2 counts being consistent with a Poisson point process, P_i^{Pois} , shown as red circles; and probability $P_i^{\text{KS}}(\phi_i)$ for the ϕ_i clustering model proposed here (§2.3.1), shown as green X symbols; versus N_i , the total number of officially recorded infections for that country. The horizontal axis is logarithmic. As discussed in the text (§3.2.1), the Poisson point process is unrealistic for most of these data, while the ϕ_i clustering model is consistent with the data for most countries. Plain-text table: zenodo.4765705/phi_N_full.dat.

183 from 180 countries, yielding scores on six general criteria of media freedom and a weighted
 184 score representing executions, imprisonments, kidnappings and related abuses against journalists
 185 (Reporters sans frontières, 2021). The scores are combined into an overall score from zero (best) to
 186 100 (worst) that we denote here as PFI^{2020} .

187 In the absence of artificial interference in the SARS-CoV-2 daily counts, there is no obvious reason
 188 why media freedom should relate to the noise in the SARS-CoV-2 counts. However, a correlation be-
 189 tween the lack of media freedom and the publication of manipulated data by government agencies would
 190 not be surprising. Governments and the public service as organisations, and the individuals that compose
 191 them, are under more pressure to be honest in places and epochs where there is more press freedom. To
 192 see if the hypothesis of artificial interference is credible, the results of the current work are compared
 193 with PFI^{2020} , as published for 2020⁴, in §3.3.

194 2.3 Primary analysis

195 2.3.1 Poissonian and ϕ'_i models: full sequences

196 We first consider the full count sequence $\{n_i(j), 1 \leq j \leq T_i\}$ for each country i , with T_i valid days of
 197 analysis as defined in §2.1. Our one-parameter model assumes that the counts are predominantly grouped
 198 in clusters, each with ϕ'_i infections per cluster. Thus, the daily count $n_i(j)$ is assumed to consist of
 199 $n_i(j)/\phi'_i$ infection events. We assume that $n_i(j)/\phi'_i$ on a given day is drawn from a Poisson distribution
 200 of mean $\hat{\mu}_i(j)/\phi'_i$. We set $\hat{\mu}_i(j)$ to the median of the 4 neighbouring days, excluding day j and centred on
 201 it. For the initial sequence of 2 days, $\hat{\mu}_i(j)$ is set to $\hat{\mu}_i(3)$, and $\hat{\mu}_i(j)$ for the final 2 days is set to $\hat{\mu}_i(T_i - 2)$.
 202 By modelling $\hat{\mu}_i$ as a median of a small number of neighbouring days, our model is almost identical to
 203 the data itself and statistically robust, with only mild dependence on the choices of parameters. This
 204 definition of a model is more likely to bias the resulting analysis towards underestimating the noise on
 205 scales of several days rather than overestimating it; this method will not detect oscillations on the time
 206 scale of a few days to a fortnight that are related to the SARS-CoV-2 incubation time (Lauer et al., 2020;
 207 Yang et al., 2020; Huang et al., 2020a). For any given value ϕ'_i , we calculate the cumulative probability
 208 P'_{ij} that $n_i(j)/\phi'_i$ is drawn from a Poisson distribution of mean $\hat{\mu}_i(j)/\phi'_i$. For country i , the values P'_{ij}
 209 should be drawn from a uniform distribution if the model is a fair approximation. In particular, for ϕ'_i
 210 set to unity, P'_{ij} should be drawn from a uniform distribution if the intrinsic data distribution is Poissonian.
 211 Individual values of P'_{ij} (those that are close to zero or one) could, in principle, be used to identify
 212 individual days that are unusual, but here we do not consider these further.

213 We allow a wide logarithmic range in values of ϕ'_i , allowing the unrealistic subrange of $\phi'_i < 1$, and
 214 find the value ϕ_i that minimises the Kolmogorov–Smirnov (KS) distance (Kolmogorov, 1933; Smirnov,

⁴<https://rsf.org/en/ranking/2020>, downloaded 4 May 2021

215 1948; Justel et al., 1997; Marsaglia et al., 2003) from a uniform distribution, i.e. that maximises the KS
 216 probability that the data are consistent with a uniform distribution, when varying ϕ'_i . The one-sample KS
 217 test is a non-parametric test that compares a data sample with a chosen theoretical probability distribution,
 218 yielding the probability that the sample is drawn randomly from the theoretical distribution. This test uses
 219 information from the whole of the reconstructed cumulative distribution function, i.e. the set of P'_{ij} values
 220 for a given country i . We label the corresponding KS probability as P_i^{KS} . We write $P_i^{\text{Pois}} := P_i^{\text{KS}}(\phi'_i = 1)$
 221 to check if any country's daily infection rate sequence is consistent with Poissonian, although this is
 222 likely to be rare, as stated above: super-Poissonian behaviour seems reasonable. Of particular interest
 223 are countries with low values of ϕ_i . Allowing for a possibly fractal or other power-law nature of the
 224 clustering of SARS-CoV-2 infection counts, we consider the possibility that the optimal values ϕ_i may
 225 be dependent on the total infection count N_i . We investigate the (ϕ_i, N_i) distribution and see whether a
 226 scaling type relation exists, allowing for a corrected statistic ψ_i to be defined in order to highlight the
 227 noise structure of the counts independent of the overall scale N_i of the counts.

228 Standard errors in ϕ_i for a given country i are estimated once ϕ_i has been obtained by assuming
 229 that $\hat{\mu}_i(j)$ and ϕ_i are correct and generating 30 Poisson random simulations of the full sequence for that
 230 country. Since the scales of interest vary logarithmically, the standard deviation of the best estimates of
 231 $\log_{10} \phi_i$ for these numerical simulations is used as an estimate of $\sigma(\log_{10} \phi_i)$, the logarithmic standard
 232 error in ϕ_i .

233 **2.3.2 Subsequences**

234 Since artificial interference in daily SARS-CoV-2 infection counts for a given country might be restricted
 235 to shorter periods than the full data sequence, we also analyse 28-, 14- and 7-day subsequences. These
 236 analyses are performed using the same methods as above (§2.3.1), except that the 28-, 14- or 7-day
 237 subsequence that minimises ϕ_i is found. The search over all possible subsequences would require calcu-
 238 lation of a Šidák-Bonferonni correction factor (Abdi, 2007) to judge how anomalous they are. The KS
 239 probabilities that we calculate need to be interpreted keeping this in mind. Since the subsequences for a
 240 given country overlap, they are clearly not independent from one another. Instead, the *a posteriori* inter-
 241 pretation of the results of the subsequence searches found here should at best be considered indicative of
 242 periods that should be considered interesting for further verification.

243 **2.4 Alternative analyses**

244 Alternatives to the method presented in §2.3.1 are checked to see if they provide better models of the
 245 data.

246 **2.4.1 Logarithmic median model**

247 Each country's time series is by default modelled with the mean of the expected Poisson distribution
 248 for $n_i(j)/\phi'_i$ on a given day being $\hat{\mu}_i(j)/\phi'_i$, where $\hat{\mu}_i(j)$ is the median of n_i in the 4 neighbouring
 249 days, excluding day j and centred on it. As an alternative, we replace $\hat{\mu}_i(j)$ on day j by $\hat{v}_i(j) :=$
 250 $\exp(\text{median}(\ln(n_i)))$ calculated over the same set of neighbouring days. That is, we replace the usual
 251 linear median by a logarithmic median. This might better model the growing and decaying exponential
 252 phases of the infection count sequence.

253 **2.4.2 Negative binomial model**

The negative binomial distribution forbids underdispersion, but is worth considering, given its epidemi-
 ological motivation for the step from primary to secondary infections (Lloyd-Smith et al., 2005; Endo
 et al., 2020; He et al., 2020). For the counts of a given country i , we define an overdispersion parameter
 ω'_i , where the binomial probability mass function for a given infection count k , considered as k 'failures',
 compared to r 'successes', with a probability p of success, is

$$P(k; n, p) = \binom{k+r-1}{k} (1-p)^k p^r$$

$$p := \frac{\omega'_i}{1 + \omega'_i}. \tag{1}$$

\tag{2}

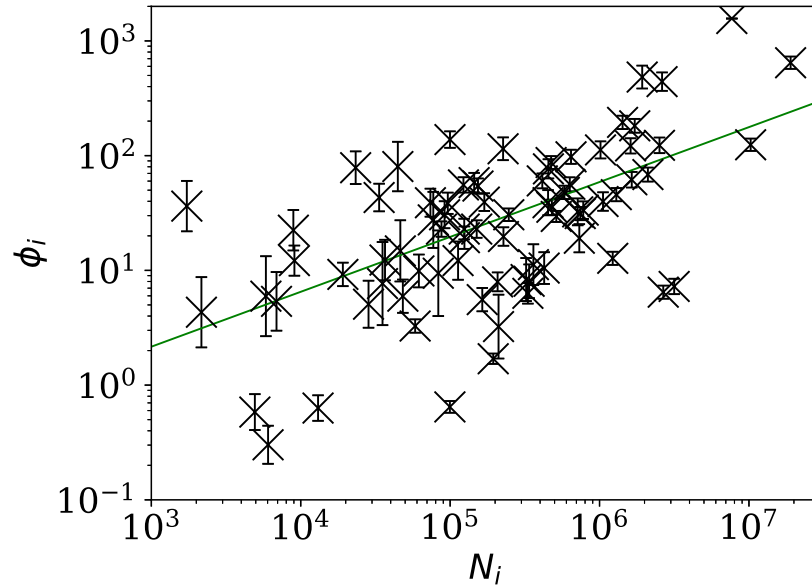


Figure 3. Noisiness in daily SARS-CoV-2 counts, showing the clustering parameter ϕ_i (§2.3.1) that best models the noise, versus the total number of counts for that country N_i . The error bars show standard errors derived from numerical simulations based on the model. The axes are logarithmic, as indicated. Values of the clustering parameter ϕ_i below unity indicate sub-Poissonian behaviour – the counts in these cases are less noisy than expected for Poisson statistics. A robust (Theil, 1950; Sen, 1968) linear fit of $\log_{10} \phi_i$ against $\log_{10} N_i$ is shown as a thick green line (§3.2.1). Plain-text table: [zenodo.4765705/phi_N_full.dat](https://zenodo.org/record/4765705/files/phi_N_full.dat).

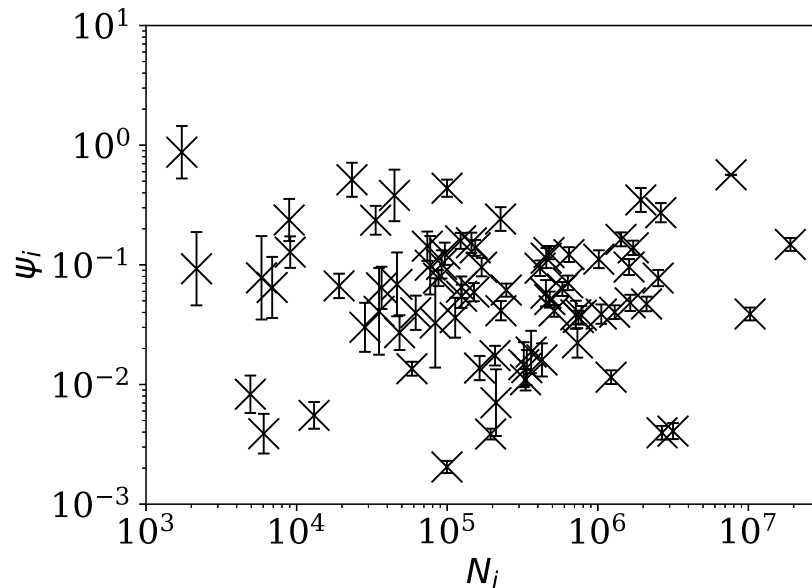


Figure 4. Normalised noisiness ψ_i (Eq. (7)) for daily SARS-CoV-2 counts versus total counts N_i . The error bars are as in Fig. 3, assuming no additional error source contributed by N_i . The axes are logarithmic. Several low ψ_i values appear to be outliers of the ψ_i distribution.

On day j , with a modelled count of $\hat{\mu}_i(j)$, we set

$$r := \omega_i' \hat{\mu}_i(j), \quad (3)$$

254 giving $\hat{\mu}_i(j)$ as the mean of the distribution and $\hat{\mu}_i(j)(1 + \omega_i')$ as the variance. The preferred value of
 255 ω_i' (that yielding the lowest Kolmogorov–Smirnov test statistic when comparing the set of cumulative
 256 probabilities with a uniform distribution, as in §2.3.1) is then ω_i . Thus, ω_i should behave similarly to ϕ_i
 257 to represent typical cluster size when both are greater than unity, while at low values (below unity), ω_i
 258 will be unable to represent distributions that are underdispersed with respect to the Poisson distribution,
 259 and will instead rapidly approach zero (the Poisson limit).

260 **2.4.3 Does anti-clustering exist in grouped data?**

261 The temptation to make ‘unnoticeable’ modifications that hide an increase in data from day j to day $j + 1$
 262 might be less likely to occur on greater timescales. Moreover, some of the phenomena contributing to the
 263 intrinsic and administrative components of ϕ_i' should be independent of time scale, while others should
 264 depend on the time scale. To provide clues for this type of analysis, the $n_i(j)$ data have been summed in
 265 pairs and triplets of days, ignoring any one- or two-day remainder at the end of a sequence. These were
 266 analysed using the same algorithm as above for the full sequences (§2.3.1).

267 **2.4.4 Akaike and Bayesian information criteria**

In each case we calculate the Akaike (1974) and Bayesian (Schwarz, 1978) information criteria, defined

$$\text{AIC} := 2k - 2 \sum_i \ln L_i \quad (4)$$

$$\text{BIC} := \ln(N^{\text{days}}) k - 2 \sum_i \ln L_i, \quad (5)$$

$$(6)$$

268 respectively. The number of free parameters k is defined as the number of countries satisfying the criteria
 269 for a sequence to be analysable (§2.1), since there is one free parameter allowed to vary individually for
 270 each country. The number of data points for BIC is set to the total number of days N^{days} in the sequences
 271 over all k countries. The ϕ_i' model, and the logarithmic median and negative binomial alternatives, each
 272 have the same values of k and N^{days} . The 2-day and 3-day alternatives can be expected to have slightly
 273 smaller numbers of countries k whose sequences satisfy the analysis criteria, and much smaller numbers
 274 N^{days} of ‘days’, since in reality these no longer represent single days. The maximum likelihood is
 275 defined $L_i := P_i^{\text{KS}}$, i.e. the Kolmogorov–Smirnov probability that the observed values for the country are
 276 drawn from a rescaled Poisson (or negative binomial) distribution, as defined above.

277 **3 RESULTS**

278 **3.1 Data**

279 The 139 countries and territories in the C19CCTF counts data have 27 negative values out of the total
 280 of 36445 values. These can reasonably be interpreted as corrections for earlier overcounts, and we reset
 281 these values to zero, with a negligible reduction in the amount of data. Consecutive sequences of days
 282 satisfying the criteria listed in §2.1 were found for $M^{\text{valid}} = 78$ countries.

283 **3.2 Clustering of SARS-CoV-2 counts**

284 **3.2.1 Full infection count sequences**

285 Figure 2 shows, unsurprisingly, that only a small handful of the countries’ daily SARS-CoV-2 counts
 286 sequences have noise whose statistical distribution is consistent with the Poisson distribution, in the
 287 sense modelled here: P_i^{Poiss} (red circles) is close to zero in most cases. Specifically, 63 countries (80.8%)
 288 are inconsistent with the Poisson distribution at a significance of $P_i^{\text{Poiss}} < 0.01$ and 66 countries (84.6%)
 289 are non-Poissonian at $P_i^{\text{Poiss}} < 0.05$. On the contrary, the introduction of the ϕ_i' parameter, optimised
 290 to ϕ_i for each country i , provides a sufficiently good fit in most cases, especially for the countries with
 291 low clustering ϕ_i . While some of the probabilities ($P_i^{\text{KS}}(\phi_i)$, green x symbols) in Fig. 2 are low in
 292 countries with the highest numbers of infections, these countries also have high ϕ_i , so are not of interest
 293 as indicators of the absence of noise. Among countries with $\phi_i < 10.0$, the lowest probability P_i^{KS} is

Table 1. Clustering parameters for the countries with the 10 lowest ϕ_i and 10 lowest ψ_i values, i.e. the least noise; extended version of table: zenodo.4765705/phi_N_full.dat.

country	ϕ'_i model					alternative analyses			
	N_i	P_i^{Poiss}	P_i^{KS}	ϕ_i	ψ_i	\hat{v}_i	ω_i	P_i^{KS}	ω_i
Nicaragua	6046	0.17	0.77	0.30	0.003	0.66	0.30	0.17	0.00
Syria	4931	0.29	0.92	0.58	0.008	0.92	0.58	0.29	0.00
Tajikistan	13062	0.17	0.76	0.63	0.005	0.78	0.67	0.16	0.00
Algeria	99610	0.01	0.17	0.65	0.002	0.13	0.62	0.01	0.00
Belarus	194284	0.01	0.53	1.70	0.003	0.40	1.57	0.46	0.58
Croatia	210837	0.27	0.89	3.24	0.007	0.89	3.24	0.70	1.02
Albania	58316	0.00	0.44	3.27	0.013	0.41	3.27	0.30	1.80
New Zealand	2164	0.44	0.90	4.32	0.092	0.94	4.32	0.86	1.19
Australia	28430	0.11	0.90	5.07	0.030	0.90	5.69	0.87	3.55
Thailand	6884	0.29	0.99	5.37	0.064	0.99	5.37	0.96	3.80
Algeria	99610	0.01	0.17	0.65	0.002	0.13	0.62	0.01	0.00
Belarus	194284	0.01	0.53	1.70	0.003	0.40	1.57	0.46	0.58
Nicaragua	6046	0.17	0.77	0.30	0.003	0.66	0.30	0.17	0.00
Turkey	2669568	0.00	0.20	6.46	0.003	0.16	6.09	0.16	5.07
Russia	3159297	0.00	0.24	7.24	0.004	0.19	7.08	0.22	6.03
Tajikistan	13062	0.17	0.76	0.63	0.005	0.78	0.67	0.16	0.00
Croatia	210837	0.27	0.89	3.24	0.007	0.89	3.24	0.70	1.02
Syria	4931	0.29	0.92	0.58	0.008	0.92	0.58	0.29	0.00
Saudi Arabia	331359	0.00	0.91	6.31	0.010	0.84	6.17	0.83	4.90
Iran	1225142	0.00	0.82	12.73	0.011	0.58	11.61	0.71	11.35

294 that of Algeria with $P_i^{\text{KS}} = 0.17$, i.e., the ϕ_i model is consistent with the data. In contrast, the negative
295 binomial model ϕ_i^{NB} (see §3.2.3 below), which is super-Poissonian by definition, and cannot model sub-
296 Poissonian behaviour, yields $P_i^{\text{KS}} = 0.01$ for Algeria. Consistently with this, the Poissonian model for
297 Algeria gives $P_i^{\text{Poiss}} = 0.005$. The full sequence for Algeria is only fit by the ϕ'_i model, which allows
298 sub-Poissonian behaviour.

299 The consistency of the ϕ_i model with most of the data justifies continuing to Figure 3, which clearly
300 shows a scaling relation: countries with greater overall numbers N_i of infections also tend to have greater
301 noise in the daily counts $n_i(j)$. A Theil–Sen linear fit (Theil, 1950; Sen, 1968) to the relation between
302 $\log_{10} \phi_i$ and $\log_{10} N_i$ has a zeropoint of -1.10 ± 0.44 and a slope of 0.48 ± 0.07 , where the standard errors
303 (68% confidence intervals if the distribution is Gaussian) are conservatively generated for both slope and
304 zeropoint by 100 bootstraps. By using a robust estimator, the low ϕ_i cases, which appear to be outliers,
305 have little influence on the fit. The fit is shown as a thick green line in Fig. 3.

This ϕ_i – N_i relation is consistent with $\phi_i \propto \sqrt{N_i}$. To adjust the ϕ_i clustering value to take into account
the dependence on N_i , and given that the slope is consistent with this simple relation, we propose an
empirical definition of a normalised clustering parameter

$$\psi_i := \phi_i / \sqrt{N_i}, \quad (7)$$

306 so that ψ_i should, by construction, be approximately constant. While the estimated slope of the relation
307 could be used rather than this half-integer power relation, the fixed relation in Eq. (7) offers the benefit
308 of simplicity.

This relation should not be confused with the usual Poisson error. By the divisibility of the Poisson
distribution, the relation $\phi_i \propto \sqrt{N_i}$ that was found here can be used to show that

$$\begin{aligned} \sigma[\hat{\mu}_i(j)/\phi_i] &\sim \sqrt{\hat{\mu}_i(j)/\phi_i} \\ \Rightarrow \sigma[\hat{\mu}_i(j)] &\sim \phi_i \sqrt{\hat{\mu}_i(j)/\phi_i} \propto N_i^{1/4} \hat{\mu}_i(j)^{1/2}, \end{aligned} \quad (8)$$

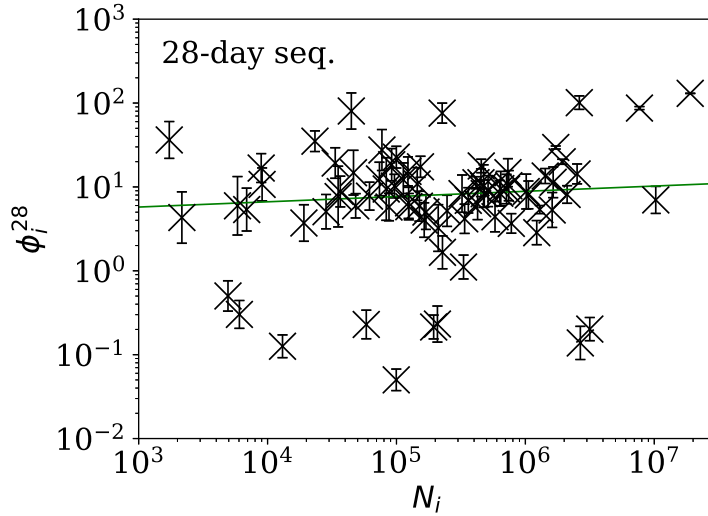


Figure 5. Clustering parameter ϕ_i^{28} for the 28-day sequence of lowest ϕ_i^{28} , as in Fig. 3. The vertical axis range is expanded from that in Fig. 3, to accommodate lower values. A robust (Theil, 1950; Sen, 1968) linear fit of $\log_{10} \phi_i^{28}$ against $\log_{10} N_i$ is shown as a thick green line (§3.2.1). Plain-text table: zenodo.4765705/phi_N_28days.dat.

where $\sigma[x]$ is the standard deviation of random variable x . If we accept $\hat{\mu}_i(j)$ as a fair model for $n_i(j)$ and that $n_i(j)$ is proportional to N_i , then we obtain

$$\sigma[n_i(j)] \propto n_i^{3/4}. \quad (9)$$

309 Figure 4 shows visually that ψ_i appears to be scale-independent, in the sense that the dependence on
 310 N_i has been cancelled, by construction. The countries with the 10 lowest values of ψ_i are Algeria, Belarus,
 311 Nicaragua, Turkey, Russia, Tajikistan, Croatia, Syria, Saudi Arabia, and Iran. Detailed SARS-CoV-2
 312 daily count noise characteristics for the countries with lowest ϕ_i and ψ_i are listed in Table 1, including
 313 the Kolmogorov–Smirnov probability that the data are drawn from a Poisson distribution, P_i^{Poiss} , the
 314 probability of the optimal ϕ_i model, P_i^{KS} , and ϕ_i and ψ_i .

315 The approximate proportionality of ϕ_i to $\sqrt{N_i}$ for the full sequences is strong and helps separate
 316 low-noise SARS-CoV-2 count countries from those following the main trend. However, the results for

Table 2. Least noisy 28-day sequences – clustering parameters for the countries with the 10 lowest ϕ_i^{28} values; extended table: zenodo.4765705/phi_N_28days.dat.

country	N_i	$\langle n_i^{28} \rangle$	P_i^{Poiss}	P_i^{KS}	ϕ_i^{28}	starting date
Algeria	99610	227.6	0.00	0.36	0.05	2020-09-03
Tajikistan	13062	63.0	0.02	0.96	0.13	2020-06-07
Turkey	2669568	1014.5	0.03	1.00	0.14	2020-06-30
Russia	3159297	5403.8	0.26	0.59	0.20	2020-07-20
Belarus	194284	921.9	0.14	0.89	0.21	2020-05-08
Albania	58316	203.8	0.33	0.64	0.23	2020-09-27
United Arab Emirates	207822	512.8	0.08	0.23	0.23	2020-04-14
Nicaragua	6046	135.7	0.17	0.77	0.30	2020-07-07
Syria	4931	70.0	0.19	0.91	0.50	2020-08-15
Saudi Arabia	331359	1182.2	0.47	0.54	1.11	2020-04-12

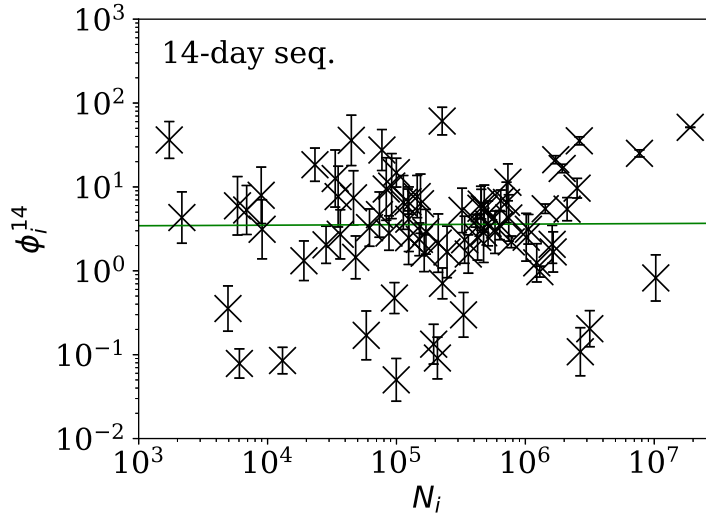


Figure 6. Clustering parameter ϕ_i^{14} for the 14-day sequence of lowest ϕ_i^{14} , as in Fig. 5. Plain-text table: zenodo.4765705/phi_N_14days.dat.

317 subsequences shown below in §3.2.2 suggest that this N_i dependence may be an effect of the typically
 318 longer durations of the pandemic in countries where the overall count is higher.

3.2.2 Subsequences of infection counts

319 Figures 5–7 show the equivalent of Fig. 3 for sequences of lengths 28, 14 and 7 days, respectively.
 320 The Theil–Sen robust fits to the logarithmic (ϕ_i^{28}, N_i) ; (ϕ_i^{14}, N_i) ; and (ϕ_i^7, N_i) relations are zeropoints
 321 and slopes of 0.57 ± 0.43 and 0.06 ± 0.08 ; 0.52 ± 0.47 and 0.01 ± 0.09 ; and -0.10 ± 0.83 and $0.02 \pm$
 322 0.13 , respectively. There is clearly no significant dependence of ϕ_i^d on N_i for any of these fixed length
 323 subsequences, in contrast to the case of the ϕ_i dependence on N_i for the full count sequences. Thus,
 324 the empirical motivation for using ψ_i (Eq. (7)) to discriminate between the countries’ full sequences of
 325 SARS-CoV-2 data is not justified from the information gained from the subsequences alone. Tables 2–4
 326 show the countries with the least noisy sequences as determined by ϕ_i^{28} , ϕ_i^{14} and ϕ_i^7 , respectively.
 327

328 Tables 2 and 3 show that the lists of countries with the strongest anti-clustering are similar to one
 329 another. Thus, Fig. 8 shows the SARS-CoV-2 counts curves for countries with the lowest ϕ_i^{28} , and Fig. 9
 330 the curves for those with the lowest ϕ_i^7 . Both figures exclude countries with total counts $N_i \leq 10000$, in

Table 3. Least noisy 14-day sequences – clustering parameters for the countries with the 10 lowest ϕ_i^{14} values; extended version of table: zenodo.4765705/phi_N_14days.dat.

country	N_i	$\langle n_i^{14} \rangle$	P_i^{Poiss}	P_i^{KS}	ϕ_i^{14}	starting date
Algeria	99610	285.9	0.12	0.40	0.05	2020-09-01
Nicaragua	6046	73.6	0.12	0.98	0.08	2020-09-22
Tajikistan	13062	64.6	0.02	0.99	0.09	2020-06-11
United Arab Emirates	207822	521.2	0.11	0.56	0.09	2020-04-19
Turkey	2669568	971.6	0.12	0.86	0.11	2020-07-08
Belarus	194284	945.6	0.22	1.00	0.13	2020-05-12
Albania	58316	143.4	0.21	0.96	0.17	2020-09-01
Russia	3159297	5627.0	0.47	0.98	0.20	2020-07-21
Saudi Arabia	331359	1227.5	0.38	0.96	0.30	2020-04-19
Syria	4931	76.6	0.42	0.96	0.35	2020-08-14

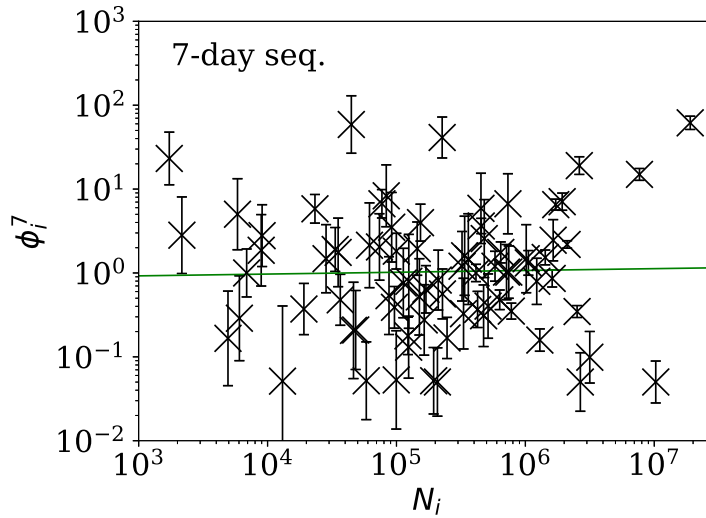


Figure 7. Clustering parameter ϕ_i^7 for the 7-day sequence of lowest ϕ_i^7 , as in Fig. 5. There are clearly a wider overall scatter and bigger error bars compared to Figs 5 and 6; a low ϕ_i^7 is a noisier indicator than ϕ_i^{28} and ϕ_i^{14} for individual countries. Plain-text table: zenodo.4765705/phi_N_07days.dat.

Table 4. Least noisy 7-day sequences – clustering parameters for the countries with the 10 lowest ϕ_i^7 values; extended table: zenodo.4765705/phi_N_07days.dat.

country	N_i	$\langle n_i^7 \rangle$	P_i^{Pois}	P_i^{KS}	ϕ_i^7	starting date
United Arab Emirates	207822	544.9	0.24	0.99	0.05	2020-04-27
India	10266674	10109.3	0.34	0.60	0.05	2020-06-06
Turkey	2669568	929.6	0.22	0.93	0.05	2020-07-15
Tajikistan	13062	51.9	0.16	0.77	0.05	2020-06-28
Albania	58316	297.7	0.23	0.98	0.05	2020-10-18
Belarus	194284	947.9	0.60	0.94	0.05	2020-05-13
Algeria	99610	204.3	0.37	0.49	0.05	2020-10-14
Russia	3159297	5076.7	0.36	0.68	0.10	2020-08-09
Ethiopia	124264	456.7	0.83	0.93	0.13	2020-12-13
Poland	1294878	297.7	0.31	0.96	0.16	2020-06-20

Table 5. Akaike (1974) and Bayesian (Schwarz, 1978) information criteria for the ϕ_i^7 and alternative analyses; plain-text version: zenodo.4765705/AIC_BIC_full.dat.

model	ϕ_i^7		log. median		neg. binomial		2-day grouping		3-day grouping	
	AIC	BIC	AIC	BIC	AIC	BIC	AIC	BIC	AIC	BIC
	268.60	848.87	289.91	870.18	377.52	957.79	313.21	878.50	208.49	743.75

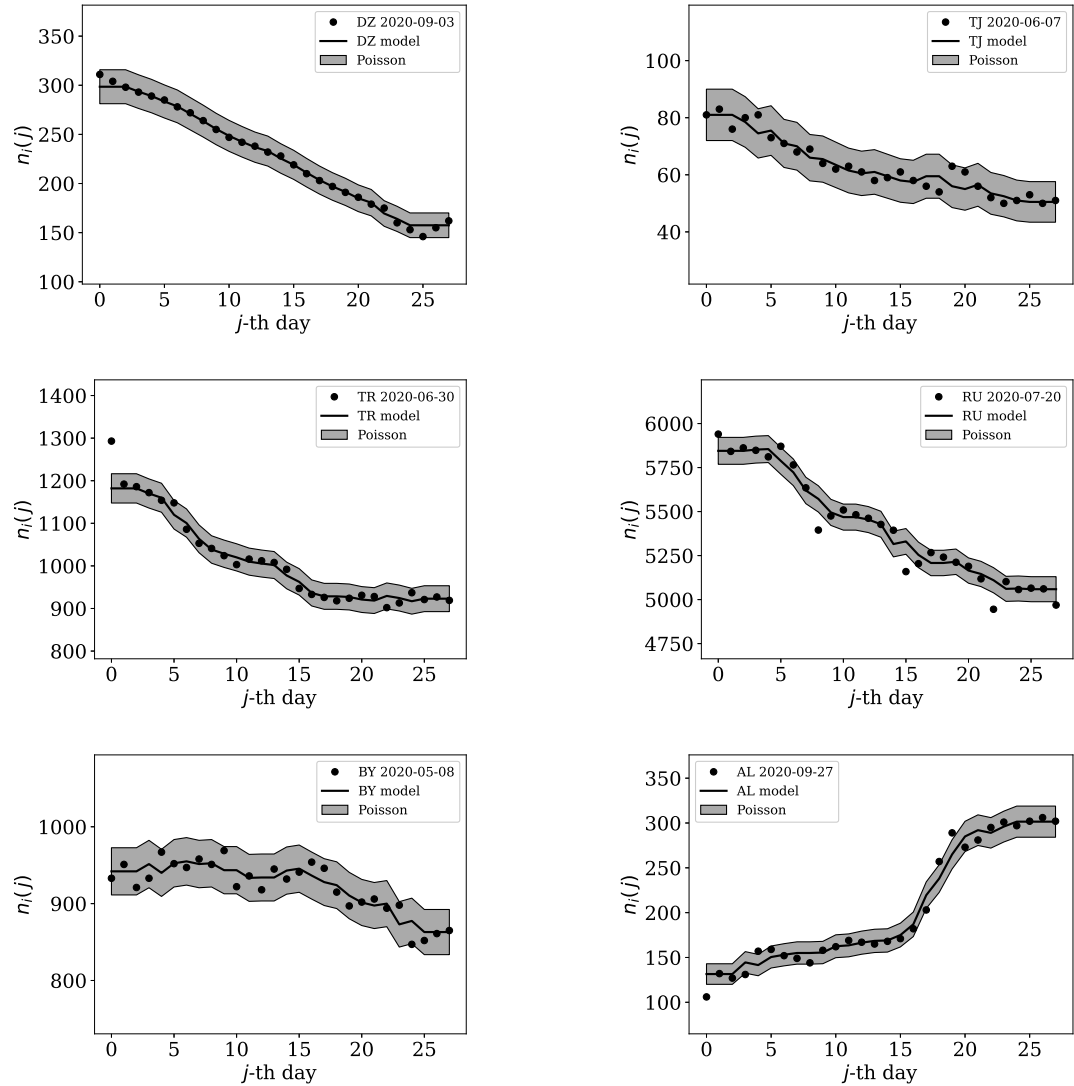


Figure 8. Least noisy 28-day official SARS-CoV-2 national daily counts for countries with total counts $N_i > 10000$ (see Fig. 5 and Table 2), shown as dots in comparison to the $\hat{\mu}_i(j)$ model (median of the 4 neighbouring days) and 68% error band for the Poisson point process. The ranges in daily counts (vertical axis) are chosen automatically and in most cases do not start at zero. About nine (32%) of the points should be outside of the shaded band unless the counts have an anti-clustering effect that weakens Poisson noise. The dates indicate the start date of each sequence. ISO-3166-1 key: DZ: Algeria, TJ: Tajikistan, TR: Turkey, RU: Russia, BY: Belarus, AL: Albania.

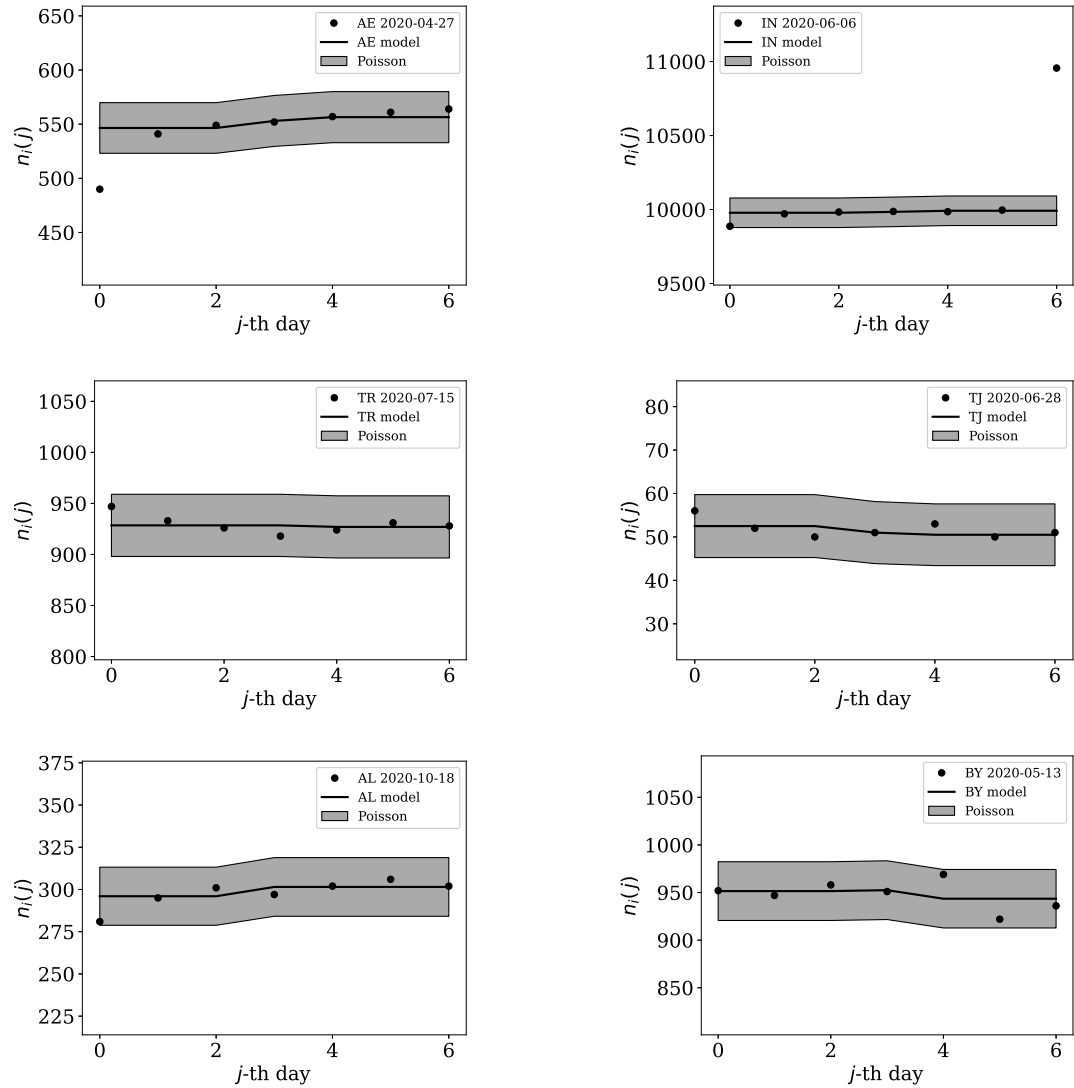


Figure 9. Least noisy 7-day daily counts for countries with total counts $N_i > 10000$ (see Fig. 7 and Table 4), as in Fig. 8. A concentration of points close to the model indicates an anti-clustering effect; about 68% (five) of the points should scatter up and down throughout the shaded band if the counts are Poissonian, and about 32% (two) should be outside the band. In several cases, the data points appear to be mostly stuck to the model, with almost no scatter. ISO-3166-1 key: AE: United Arab Emirates, IN: India, TR: Turkey, TJ: Tajikistan, AL: Albania, BY: Belarus.

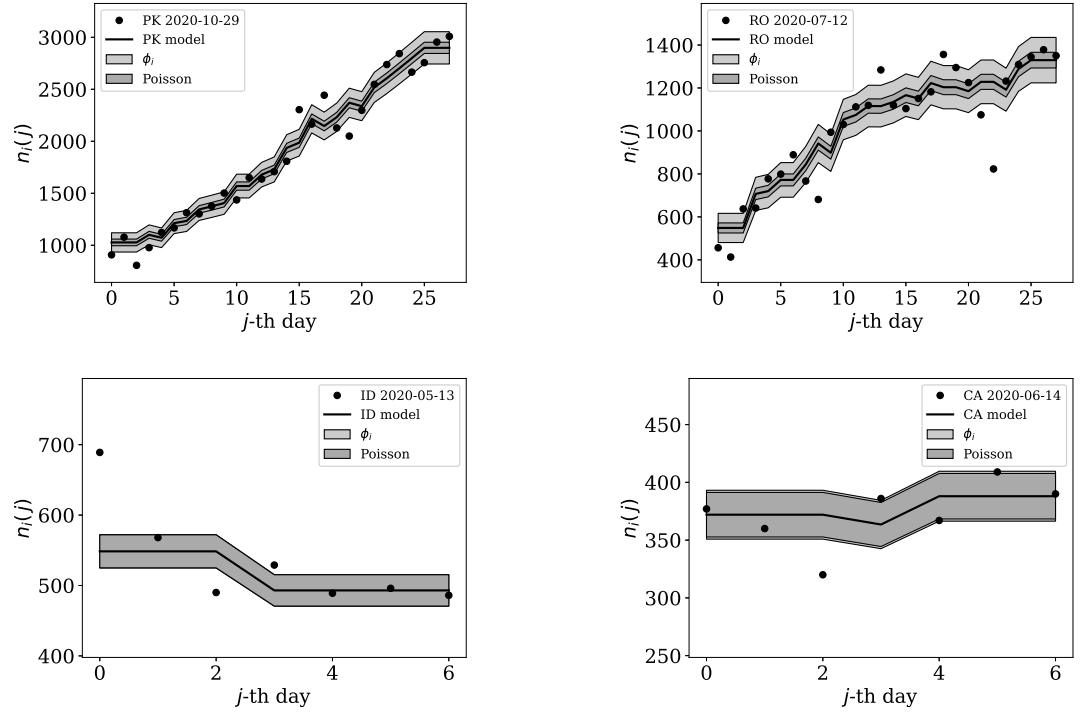


Figure 10. Typical (median) 28-day (above) and 7-day (below) daily counts, as in Figs 8 and 9. The dark shaded band again shows a Poissonian noise model, which underestimates the noise. A faint shaded band shows the ϕ_i models for these countries' SARS-CoV-2 daily counts, and should contain about 68% of the infection count points. ISO-3166-1 key: PK: Pakistan, RO: Romania, ID: Indonesia, CA: Canada.

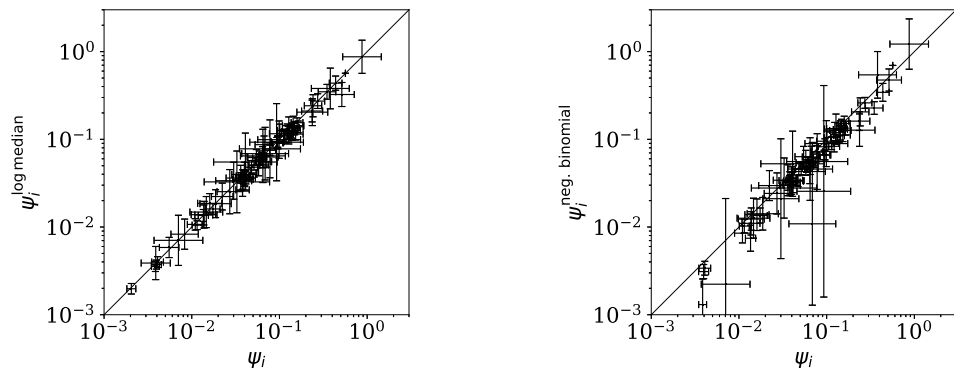


Figure 11. *Left:* Normalised clustering parameter ψ_i^{LM} (Eq. (7)) using the logarithmic median model of the expected full-sequence counts (§2.4.1) versus ψ_i for the primary analysis. *Right:* Normalised clustering $\psi_i^{\text{NB}} := \omega_i / \sqrt{N_i}$ for the negative binomial model (see Eqs (2), (3)) versus ψ_i . A line shows $\psi_i^{\text{LM}} = \psi_i$ and $\psi_i^{\text{NB}} = \psi_i$, respectively. The data point for Algeria, with $\log_{10} \psi_i = -2.69 \pm 0.05$, $\log_{10} \psi_i^{\text{NB}} = -5.69 \pm 0.93$, lies below the displayed area in the right-hand panel. Plain-text table: [zenodo.4765705/phi_N_full.dat](https://zenodo.org/record/4765705/files/phi_N_full.dat).

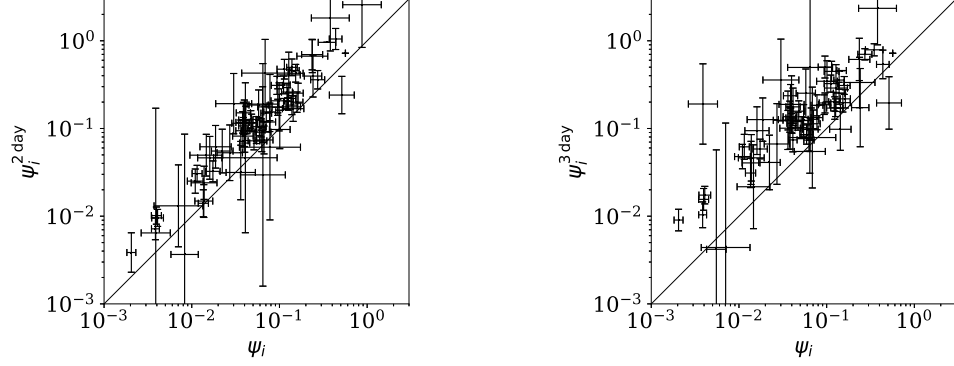


Figure 12. Normalised noisiness ψ_i^{2d} and ψ_i^{3d} (Eq. (7)) for counts summed in successive pairs (*left*) and triplets (*right*) of days, respectively, versus that for the primary analysis. A line shows $\psi_i^{2d} = \psi_i$ and $\psi_i^{3d} = \psi_i$, respectively. Plain-text table: zenodo.4765705/phi_N_full.dat.

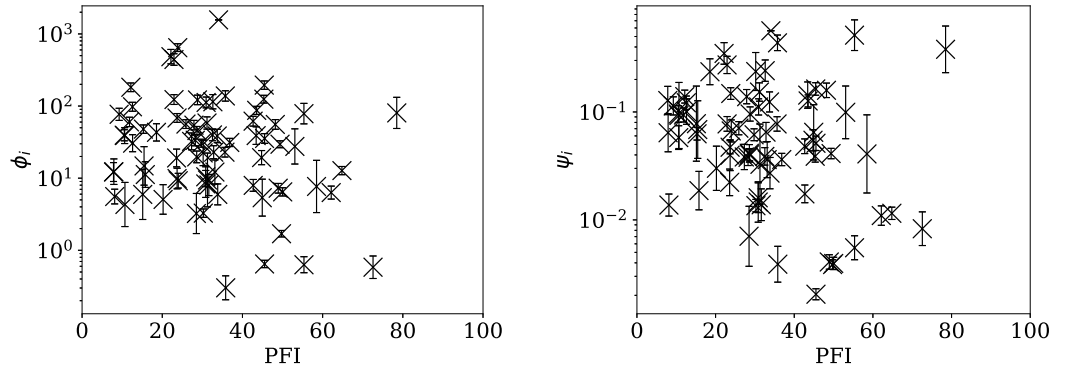


Figure 13. Dependence of ϕ_i (*left*) and ψ_i (*right*) on the Press Freedom Index (PFI^{2020}) for the full sequences.

331 which low total counts tend to give low clustering. It is clear in these figures that several countries have
 332 subsequences that are strongly sub-Poissonian – with some form of anti-clustering, whether natural or
 333 artificial.

334 Countries in the median of the ϕ_i^{28} and ϕ_i^7 distributions have their curves shown in Fig. 10 for com-
 335 parison. It is visually clear in the figure that the counts are dispersed widely beyond the Poissonian band,
 336 and that the ϕ_i^{28} and ϕ_i^7 models are reasonable as a model for representing about 68% of the counts
 337 within one standard deviation of the model values.

338 **3.2.3 Alternative analyses**

339 Figure 11 (*left*) shows that the logarithmic median model (§2.4.1) of the counts gives almost identical
 340 best estimates to those of the primary model, i.e. $\psi_i^{\text{LM}} \approx \psi_i$, but Table 5 shows very strong evidence
 341 favouring the original, arithmetic median model.

342 Figure 11 (*right*) shows that the negative binomial model (§2.4.2) roughly gives $\psi_i^{\text{NB}} \sim \psi_i$ (i.e. $\omega_i \sim$
 343 ϕ_i), tending to $\psi_i^{\text{NB}} < \psi_i$, especially for the least clustered cases. The error bars are very big for ψ_i^{NB}
 344 for several countries. Table 5 again shows very strong evidence favouring the original model over the
 345 negative binomial model.

346 Figure 12 shows that the counts grouped (summed) in pairs and triplets (§2.4.3) yield ψ_i^{2d} and ψ_i^{3d}
 347 with more scatter and generally larger error bars than that of ψ_i , and ψ_i^{2d} and ψ_i^{3d} are mostly greater than
 348 ψ_i . Whether the AIC and BIC evidence (Table 5) for 2-day and 3-day grouped data can be directly com-
 349 pared to that of the main analysis depends on whether the grouped data can be considered to be the same
 350 observational data as the original data, modelled with fewer free parameters. Since the characteristic of

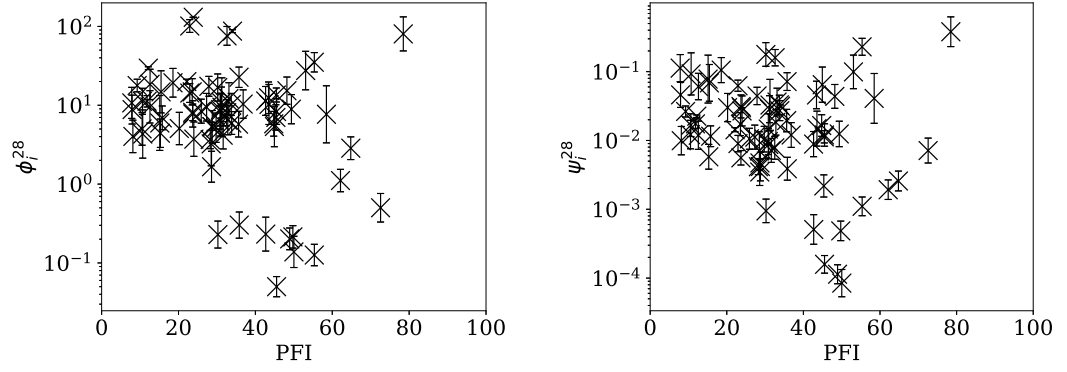


Figure 14. Dependence of ϕ_i^{28} (left) and ψ_i^{28} (right) on PFI^{2020} for the 28-day subsequences.

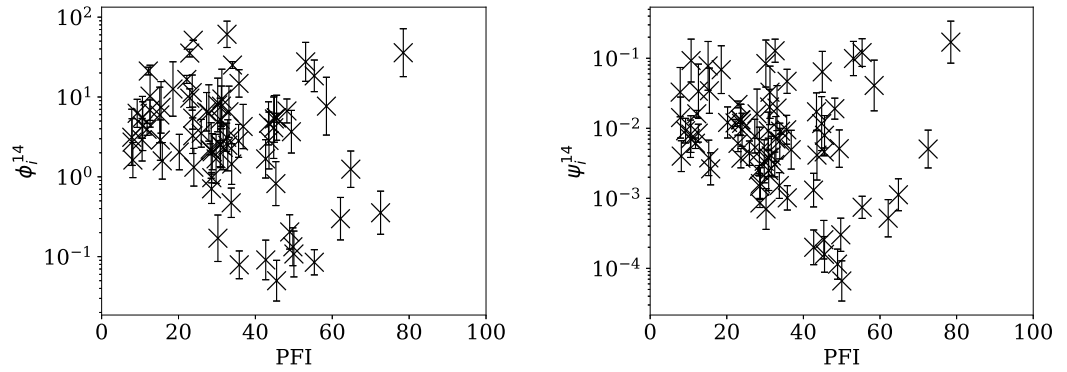


Figure 15. Dependence of ϕ_i^{14} (left) and ψ_i^{14} (right) on PFI^{2020} for the 14-day subsequences.

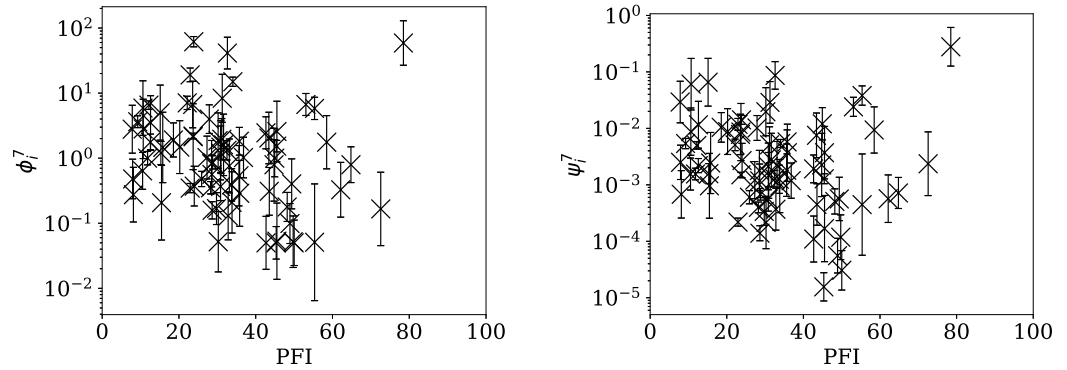


Figure 16. Dependence of ϕ_i^7 (left) and ψ_i^7 (right) on PFI^{2020} for the 7-day subsequences.

Table 6. Kendall τ statistic and its significance (two-sided) P^τ for the null hypothesis of no correlation between the ranking of PFI^{2020} and ϕ_i or ψ_i for the full data or subsequences; plain-text version: [zenodo.4765705/pfi_correlations_table.dat](https://zenodo.org/record/4765705/files/pfi_correlations_table.dat).

parameter	full		28-day		14-day		7-day	
	τ	P^τ	τ	P^τ	τ	P^τ	τ	P^τ
ϕ_i	-0.118	0.131	-0.126	0.108	-0.148	0.0584	-0.200	0.0108
ψ_i	-0.160	0.0408	-0.157	0.0445	-0.176	0.0249	-0.170	0.0300

351 study is the noise, not the signal, the validity of this direct comparison is doubtful. Nevertheless, if the
352 values of the AIC and BIC evidence are considered literally, then the 2-day grouping would yield a worse
353 model than the model of the daily data, while the 3-day grouping would yield a better model than that for
354 the daily data. The comparison of these different analyses could potentially be used to obtain a deeper
355 understanding of the complex dynamics of this pandemic. The epidemiologically relevant sociological
356 parameters of countries around the world are highly diverse (varying in population density, patterns of
357 social contact, tendency to obey or disobey official health guidelines such as lockdown measures, de-
358 mographic profiles, quality and availability of health services, communication patterns, frequency of
359 COVID-19 comorbidity conditions, climate (Afshordi et al., 2020)), so comparison of the clustering
360 behaviour on these different time scales might help to separate out some of these contributions.

361 **3.3 Comparison with the RSF Press Freedom Index**

362 Figures 13–16 show the relation between ϕ_i and ψ_i and the RSF Press Freedom Index (PFI²⁰²⁰; §2.2) for
363 the full sequences and subsequences. Table 6 non-parametrically tests for correlations in these relations
364 using the Kendall rank correlation statistic τ (Kendall, 1938, 1970; Croux & Dehon, 2010). The first row
365 of the table shows that the unnormalised clustering parameter ϕ_i for the full sequence and subsequences
366 generally anticorrelates with PFI²⁰²⁰. The strongest case is for 7-day subsequences, in which case the
367 anticorrelation is significant at $P^\tau = 0.0108$.

368 The normalised clustering parameter ψ_i was found to be necessary above (Eq. (7)) to remove depen-
369 dence on the total infection scale N_i in the full sequences. The second row of Table 6 shows that for ψ_i ,
370 the anticorrelation is significant at the $P^\tau < 0.05$ level for the full sequence ($P^\tau = 0.0408$) and for all the
371 subsequences. However, the analysis of the subsequence results (§3.2.2) only justifies considering ψ_i as
372 the preferred parameter for the full sequence, and using ϕ_i^{28} , ϕ_i^{14} , and ϕ_i^7 for the subsequences. Together,
373 ψ_i , ϕ_i^{28} , ϕ_i^{14} , and ϕ_i^7 yield a median significance level of $P^\tau = 0.0496 < 0.05$ (the significance is stronger
374 in the JHU CSSE data; see Table 12 in Appendix A). Thus, there is statistically significant evidence that
375 the worse the press freedom is in a country (as measured by higher PFI²⁰²⁰), the more likely it is that the
376 SARS-CoV-2 daily counts are best modelled as sub-Poissonian.

377 This result is an anticorrelation; it is not proof of a causal relation. Nevertheless, a simple explanation
378 of the observed relation would be that there is interference in the data in association with a lack of media
379 freedom.

380 **4 DISCUSSION**

381 Figures 3–7 vary in the degree to which they separate some groups of countries as being unusual in terms
382 of the characteristics of their location in the (N_i, ψ_i) plane. On visual inspection, Fig. 5, for ϕ_i^{28} , appears
383 to show the sharpest division between the main relation between clustering and total infection count, in
384 which nine countries appear to have sub-Poissonian preferred models in a group well-separated from the
385 others. If we interpret the sub-Poissonian behaviour as a result of interference associated with the lack
386 of media freedom (high PFI²⁰²⁰, §3.3, Table 6), then the more significant results are those for ϕ_i^7 (Fig. 7,
387 Table 4). If interference did occur, then other public evidence of interference might add credibility to the
388 interpretation. Here, some possible interpretations are discussed, including some individual low-noise
389 sequences in Fig. 8 and 9. Some typical sequences (as selected by median ϕ_i^{28} and ϕ_i^7) are shown for
390 comparison in Fig. 10.

391 The analysis in this paper makes very few assumptions and does not claim to measure the full na-
392 ture of the pandemic. The following interpretations of the numerical results would benefit from future
393 studies that attempt worldwide models of the underlying epidemiology of the pandemic. Detailed mod-
394 elling is usually restricted to a small number of countries (e.g. Chowdhury et al. 2020; Kim et al. 2020;
395 Molina-Cuevas 2020; Jiang, Zhao & Shao 2020; Afshordi et al. 2020).

396 **4.1 High total infection count**

397 While the main question of interest in this paper is whether anti-clustering can be detected, the results
398 may also indicate characteristics of countries with high clustering values. The United States, India and
399 Brazil are clearly separated in Figs 3 and 4 from the majority of other countries by their high official
400 total infection counts of about 10^7 . They have correspondingly higher clustering values ϕ_i , although
401 their normalised clustering values ψ_i are in the range of about $0.01 < \psi_i < 1$ covered by the majority of
402 countries in Fig. 4.

403 It does not seem realistic that the ϕ_i values greater than 600 for the US and Brazil are purely an effect
 404 of intrinsic infection events – ‘superspreader’ events in crowded places or nursing homes. While individ-
 405 ual big clusters may occur given the high overall scale of infections, it seems more likely that there is a
 406 strong role played by administrative clustering. Both countries are federations, and have numerous geo-
 407 graphic administrative subdivisions with a diversity of political and administrative methods. A plausible
 408 explanation for the dominant effect yielding $\phi_i > 600$ in these two countries is that on any individual day,
 409 the arrival and full processing of reports depends on a number of sub-national administrative regions,
 410 each reporting a few hundred new infections.

411 For example, if there are 100 reporting regions, with typically about 10 of these each reporting about
 412 600 infections daily, then typically (on about 68% of days) there will be about 7 to 13 reports per day.
 413 This would give a range varying from about 4200 to 7800 cases per day, rather than 5923 to 6077,
 414 which would be the case for unclustered, Poissonian counts (since $\sqrt{6000} \approx 77$). Lacking a system that
 415 obliges sub-national divisions – and laboratories – to report their test results in time-continuous fashion
 416 and that validates and collates those reports on a time scale much shorter than 24 hours, this type of
 417 clustering seems natural in the sociological sense. It is also possible that in these two large federations,
 418 the intrinsic heterogeneity compared to many countries of smaller populations leads to other noise effects
 419 that combine with the ‘administrative’ effect of stochasticity in the number of regional reports received
 420 as sketched above.

421 India’s overall position in the (ψ_i, N_i) plane (Fig. 4 and Table 1) appears quite typical, with an un-
 422 normalised clustering parameter $\phi_i = 124.45 \times 10^{\pm 0.054}$. However, Table 4 shows that despite its large
 423 overall infection count, India achieved a 7-day sequence with a preferred $\phi_i^7 = 0.05$, giving it a place in
 424 Table 4 and being easy to identify in the bottom-right part of Fig. 7. Figure 9 presents this subsequence.
 425 Five values appear almost exactly on the model curve rather than scattering above and below. More-
 426 over, the value is just below 10,000. Epidemiologically, it is not credible to believe that 10,000 officially
 427 reported cases per day should be an attractor resulting from the pattern of infections and system of report-
 428 ing. Given that the value of 10,000 is a round number in the decimal-based system, a reasonable specu-
 429 lation would be that the daily counts for India were artificially held at just below 10,000 for several days.
 430 The crossing of the 10,000 psychological threshold of daily infections was noted in the media (Porecha,
 431 2020), but the lack of noise in the counts during the week preceding the crossing of the threshold appears
 432 to have gone unnoticed. After crossing the 10,000 threshold, the daily infections in India continued in-
 433 creasing, as can be seen in the full counts (zenodo.4765705/WP_C19CCTF_SARSCoV2.dat).

434 4.2 Neither Poissonian nor super-Poissonian

435 The negative binomial model ϕ_i^{NB} (§3.2.3) rejects the possibility of Algeria having a super-Poissonian
 436 noise distribution at $P_i^{\text{KS}} = 0.01$. The Poissonian model for Algeria is similarly rejected with $P_i^{\text{Poiss}} =$
 437 0.005 . However, the ϕ_i model does model the Algeria data adequately, with a modest probability of
 438 $P_i^{\text{KS}} = 0.17$.

439 Figure 8 dramatically shows the least noisy 28-day sequence for Algeria. Only two days of SARS-
 440 CoV-2 recorded infections during this period appear to have diverged towards the edge of the Poissonian
 441 68% band, rather than about nine, the expected number that should be outside this band for a Pois-
 442 sonian distribution. Almost all of the points appear to stick extremely closely to the median model.
 443 It is difficult to imagine a natural process for obtaining noise that is this strongly sub-Poissonian, es-
 444 pecially in the context where most countries have super-Poissonian daily counts. Compartmental epi-
 445 demic modelling of the Algerian data, which has been published for the period ending 24 May 2020
 446 (Rouabah, Tounsi & Belaloui, 2020), could be used to try to reconstruct the true daily counts.

447 4.3 Low normalised clustering ψ_i or subsequence clustering ϕ_i^{28}, ϕ_i^{14} , or ϕ_i^7

448 4.3.1 Low clustering, high N_i

449 Turkey and Russia have total infection counts of about 3 million, similar to those of several other coun-
 450 tries, but have managed to keep their daily infection rates much less noisy – by about a factor of 10 to
 451 100 – than would be expected from the general pattern displayed in the figures. These two countries
 452 appear as an isolated pair in the bottom-right of both Figs 4 and 5, and appear in all four tables of low ψ_i
 453 (Table 1) and low subsequence ϕ_i (Tables 2–4). Russia has the very modest value of $\phi_i = 7.24 \times 10^{\pm 0.067}$
 454 and Turkey has $\phi_i = 6.46 \times 10^{\pm 0.057}$, despite their large total infection counts. This would require that
 455 both intrinsic clustering of infection events and administrative procedures work much more smoothly in

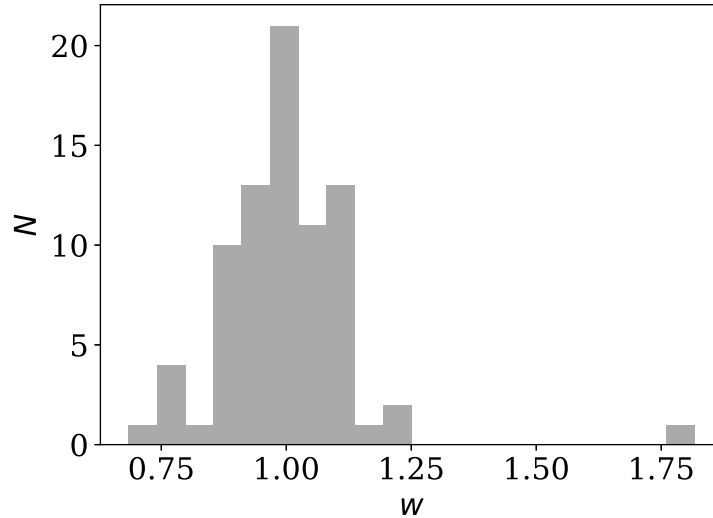


Figure 17. Histogram of weekly dip w_i (Eq. (10)) in national daily SARS-CoV-2 counts. Values below unity indicate a dip; values above unity indicate a bump. Plain-text full list of w_i : [zenodo.4765705/phi_N_full.dat](https://zenodo.org/record/4765705/files/phi_N_full.dat).

456 Russia and Turkey than in other countries with comparable total infection counts. Tables 2 and 3 and
 457 Fig. 8 show that the Russian and Turkish official SARS-CoV-2 counts indeed show very little noise compared
 458 to more typical cases (Fig. 10). There appear to be weekend dips in the Russian case (see §4.3.4
 459 below). Since these are included in the analysis, an exclusion of the weekend dips would lead to an even
 460 lower clustering estimate. At the intrinsic epidemiological level, if the Russian and Turkish counts are to
 461 be considered accurate, then very few clusters – in nursing homes, religious gatherings, bars, restaurants,
 462 schools, shops – can have occurred. Moreover, laboratory testing and transmission of data through the
 463 administrative chain from local levels to the national health agency must have occurred without the cluster-
 464 ing effects that are present in the data for the United States, Brazil, India, and other countries with high
 465 total infection counts $N_i > 2$ million, for which ϕ_i is typically above 100. International media interest in
 466 Russian COVID-19 data has mostly focussed on controversy related to COVID-19 death counts (Cole,
 467 2020), with apparently no attention given so far to the modestly super-Poissonian nature of the daily
 468 counts, in contrast to the strongly super-Poissonian counts of other countries with high total infection
 469 counts. How did Russia and Turkey achieve low- ϕ_i (super-Poissonian), i.e. low clustering?

470 **4.3.2 Low clustering, medium N_i**

471 Some cases of interest appear among the countries with officially lower total infection counts. The
 472 Belarus (BY) case is present in all four tables (Tables 1–4). The least noisy Belarusian counts curve
 473 appears in Figs 8 and 9. As with the other panels in the daily counts figures, the vertical axis is set by the
 474 data instead of starting at zero, in order to best display the information on the noise in the counts. With the
 475 vertical axis starting at zero, the Belarus daily counts would look nearly flat in this figure. They appear to
 476 be bounded above by the round number of 1000 SARS-CoV-2 infections per day, which, again, as in the
 477 case of India, could appear to be a psychologically preferred barrier. Media have expressed scepticism
 478 of Belarusian COVID-19 related data (Kramer, 2020; AFN, 2020). The Albanian case (Figs 8 and 9)
 479 also could be interpreted as hitting a psychological barrier of a decimal round number, an artificial cap
 480 of 300 infections per day, in mid-October 2020.

481 One remaining case of a coincidence is that the lowest noise 7-day sequence listed for Poland (Ta-
 482 ble 4) is for the 7-day period starting 20 June 2020, with $\phi_i^7 = 0.16 \times 10^{\pm 0.13}$. This is a factor of about
 483 300 below Poland’s clustering value for the full sequence of its SARS-CoV-2 daily infection counts,
 484 $\phi_i = 45.71 \times 10^{\pm 0.057}$, which Fig. 3 shows is typical for a country with an intermediate total infection
 485 count. On 28 June 2020, there was a *de facto* (of disputed constitutional validity, Wyrzykowski 2020;
 486 Letowska & Pacewicz 2020) first-round presidential election in Poland. Figure 9 shows that the counts

487 for Poland during the final pre-first-round-election week did not scatter widely throughout the Poissonian band. A decimal-system round number also appears in this figure: the daily infection rate is slightly
 488 above about 300 infections per day and drops to slightly below that. This appears to be the same psycho-
 489 logical daily infection count attractor as for Albania. The intrinsic clustering of SARS-CoV-2 infections
 490 in Poland together with testing and administrative clustering of the confirmed cases appear to have tem-
 491 porarily disappeared just prior to the election date, yielding what is best modelled as an incident of
 492 sub-Poissonian counts.
 493

494 **4.3.3 JHU CSSE data**

495 The JHU CSSE data give mostly similar results to the C19CCTF data. These are presented and briefly
 496 discussed in Appendix A.

497 **4.3.4 Weekend dips in the counts**

One sociological contribution to noise not mentioned above is that in several countries, the official daily
 counts are lower on or immediately after weekends. Credible factors include fewer medical and labora-
 tory workers available to carry out tests and fewer administrators registering, collecting and transmitting
 data. A dip in the counts on weekends would tend to add noise to the daily count time series, making the
 above results conservative. These dips can be quantified using the one-dimensional discrete fast Fourier
 transform (FFT). With the usual FFT convention, we transform $n_i(j)$ into $f_i(j)$ at j days, where $f_i(0)$ is
 the mean and a weekly dip should appear as a negative value at $f_i(7)$. We define a ‘weekend dip’ w_i for
 country i by subtracting the mean of the neighbours and normalising:

$$w_i := 1 + \pi \frac{f_i(7) - [f_i(6) + f_i(8)]/2}{f_i(0)}. \quad (10)$$

498 This should correspond to a multiplicative factor, i.e., $w_i = 0.85$ means a 15% dip.

499 Figure 17 shows the distribution of w_i (mean \pm std. error: 1.001 ± 0.015 ; std. dev.: 0.137; median:
 500 0.999; interquartile range: 0.104). Unexpectedly, not only are there several countries with dips, but
 501 there are also several countries with a strong *excess* signal on the 7-day time scale. There is no reason
 502 to expect the overall distribution to be Gaussian. The Shapiro–Wilk statistic (Shapiro & Wilk, 1965) is
 503 $W = 0.806$, rejecting the possibility of the distribution being Gaussian to extremely high significance:
 504 $p = 9.82 \times 10^{-9}$. Future work in studying the noise characteristics of a pandemic could take into account
 505 this weekly component of daily infection statistics.

506 **4.4 Further statistical models: autoregression**

507 A possible extension of the current work would be to iteratively consider an autoregressive model (e.g.
 508 Papoulis & Pillai, 2002, §12-3) for each time series. An initial model such as the one used here, the
 509 median of the preceding and succeeding days, could first be inferred from the sequence. This would be
 510 subtracted from the time series $n_i(j)$ to obtain a process that could be assumed as having a stationary
 511 central value and a time-varying noise distribution. An autoregressive model of the resulting sequence
 512 (or its logarithm) could then be modelled by a time-dependent (j -dependent) Poissonian or negative
 513 binomial stochastic term to find the optimal autoregression coefficients. The resulting coefficients could
 514 then be used to subtract an improved model from the times series and obtain a new iteration of an
 515 autoregression model. Continuing the iteration might lead to convergence on a specific autoregressive
 516 model that is stable against further iteration. In this case, the residual noise could then be analysed as in
 517 the current work.

518 **4.5 RSF Press Freedom Index**

519 Although the relations in Fig 13–16 generally show anticorrelations (PFI²⁰²⁰ increases from 0 to 100 as
 520 press freedom decreases, i.e. it could be better described as a lack-of-press-freedom parameter), there
 521 does appear to be a tendency for the countries with the lowest clustering values to have intermediate
 522 PFI²⁰²⁰ \sim 40. In other words, despite the overall relation, some countries with the lowest levels of press
 523 freedom appear to have noise in their daily SARS-CoV-2 counts that appears only moderately low or
 524 typical. Mainland China stands out as an exception in all eight panels of these four figures, with both a
 525 high clustering, $\phi_i = 80.35$ in the full sequence case, and a high lack of press freedom, PFI²⁰²⁰ = 78.48.

526 While a causal relation, via general processes of media freedom pressuring politicians and pub-
 527 lic servants to produce honest data, and vice versa, would provide the simplest interpretation of the

528 overall correlation found here, other interpretations should be considered. Indices to measure the
529 much wider concept of democracy tend to suffer from a lack of clarity in definitions and method
530 (Munck & Verkuilen, 2002), quite likely due to the nature of democracy as a highly complex phe-
531 nomenon that is difficult to represent with a single index. Nevertheless, Balashov et al. (2020) study
532 the relations between democracy indicators and validity in daily COVID-19 data, using a very different
533 method to the one introduced in this paper, and point out that democracy, economic and health system
534 national indicators tend to correlate strongly to one another (see §2 of Balashov et al. 2020 for a liter-
535 ature review of relations between democracy and data manipulation). An alternative interpretation to
536 direct causality could be explored along these lines. Other lines of analysis would be needed to establish
537 causal relations instead of statistical correlations.

538 5 CONCLUSION

539 Given the overdispersed, one-parameter Poissonian ϕ_i model proposed, the noise characteristics of the
540 daily SARS-CoV-2 infection data suggest that most of the countries' data form a single family in the
541 (ϕ_i, N_i) plane. The clustering – whether epidemiological in origin, or caused by testing or administrative
542 pipelines – tends to be greater for greater numbers of total infections. Several countries appear, however,
543 to show unusually anti-clustered (low-noise) daily infection counts.

544 Since these daily infection counts data constitute data of high epidemiological interest, the statistical
545 characteristics presented here and the general method could be used as the basis for further investigation
546 into the data of countries showing exceptional characteristics. The relations between the most anti-
547 clustered counts and the psychologically significant decimal system round numbers (India: 10,000 daily,
548 Belarus: 1000 daily, Albania, Poland: 300 daily), and in relation to a *de facto* national presidential
549 election, raise the question of whether or not these are just coincidences. The statistically significant
550 anticorrelation of the clustering with the *Reporters sans frontières* Press Freedom Index, i.e. less press
551 freedom was found to correlate with less clustering, strengthening the credibility of the ϕ_i clustering
552 model for judging the validity of daily pandemic data published by national government agencies. The
553 suspicious periods of data found here are mostly complementary to those studied by Balashov et al.,
554 since those authors' Benford's law analysis mainly focuses on the first-digit Benford's law during the
555 exponentially growing phases of the pandemic in any particular country (Balashov et al., 2020), while
556 this analysis studies noise in data for the full pandemic up to 6 May 2021.

557 It should be straightforward for any reader to extend the analysis in this paper by first checking
558 its reproducibility with the free-licensed source package provided using the MANEAGE framework
559 (Akhlaghi et al., 2021), and then extending, updating or modifying it in other appropriate ways; see
560 §Code availability below. Reuse of the data should be straightforward using the files archived at
561 zenodo.4765705.

562 **ACKNOWLEDGEMENTS** Thank you to Marius Peper, Taha Rouabah, Dmitry Borodaenko, anonymous col-
563 leagues, and to Niayesh Afshordi and the two other referees for several useful comments and to the Maneage
564 developers for the Maneage framework in general and for several specific comments on this work. This project has
565 been supported by the Poznań Supercomputing and Networking Center (PSNC) computational grant 314.

566 **SOFTWARE ACKNOWLEDGEMENTS** This research was partly done using the following free-licensed soft-
567 ware packages: Boost 1.73.0, Bzip2 1.0.6, cURL 7.71.1, Dash 0.5.10.2, Discoteq flock 0.2.3, Eigen 3.3.7, Expat
568 2.2.9, File 5.39, Fontconfig 2.13.1, FreeType 2.10.2, Git 2.28.0, GNU Autoconf 2.69.200-babc, GNU Automake
569 1.16.2, GNU AWK 5.1.0, GNU Bash 5.0.18, GNU Binutils 2.35, GNU Compiler Collection (GCC) 10.2.0, GNU
570 Coreutils 8.32, GNU Diffutils 3.7, GNU Findutils 4.7.0, GNU gettext 0.21, GNU gperf 3.1, GNU Grep 3.4, GNU
571 Gzip 1.10, GNU Integer Set Library 0.18, GNU libiconv 1.16, GNU Libtool 2.4.6, GNU libunistring 0.9.10, GNU
572 M4 1.4.18-patched, GNU Make 4.3, GNU Multiple Precision Arithmetic Library 6.2.0, GNU Multiple Precision
573 Complex library, GNU Multiple Precision Floating-Point Reliably 4.0.2, GNU Nano 5.2, GNU NCURSES 6.2,
574 GNU Patch 2.7.6, GNU Readline 8.0, GNU Sed 4.8, GNU Tar 1.32, GNU Texinfo 6.7, GNU Wget 1.20.3, GNU
575 Which 2.21, GPL Ghostscript 9.52, ImageMagick 7.0.8-67, Less 563, Libbsd 0.10.0, Libffi 3.2.1, libICE 1.0.10,
576 Libidn 1.36, Libjpeg v9b, Libpaper 1.1.28, Libpng 1.6.37, libpthread-stubs (Xorg) 0.4, libSM 1.2.3, Libtiff 4.0.10,
577 libXau (Xorg) 1.0.9, libxcb (Xorg) 1.14, libXdmp (Xorg) 1.1.3, libXext 1.3.4, Libxml2 2.9.9, libXt 1.2.0, Lzip
578 1.22-rc2, Metastore (forked) 1.1.2-23-fa9170b, OpenBLAS 0.3.10, Open MPI 4.0.4, OpenSSL 1.1.1a, PatchELF

579 0.10, Perl 5.32.0, pkg-config 0.29.2, Python 3.8.5, Unzip 6.0, util-Linux 2.35, util-macros (Xorg) 1.19.2, X11 li-
580 brary 1.6.9, XCB-proto (Xorg) 1.14, xorgproto 2020.1, xtrans (Xorg) 1.4.0, XZ Utils 5.2.5, Zip 3.0 and Zlib 1.2.11.
581 Python packages used include: Cyclor 0.10.0, Cython 0.29.21 (Behnel et al., 2011), Kiwisolver 1.0.1, Matplotlib
582 3.3.0 (Hunter, 2007), Numpy 1.19.1 (van der Walt et al., 2011), pybind11 2.5.0, PyParsing 2.3.1, python-dateutil
583 2.8.0, Scipy 1.5.2 (Oliphant, 2007; Millman & Aivazis, 2011), Setuptools 41.6.0, Setuptools-scm 3.3.3 and Six
584 1.12.0. L^AT_EX packages for creating the pdf version of the paper included: algorithmicx 15878 (revision), algorithms
585 0.1, biber 2.16, biblatex 3.16, bitset 1.3, booktabs 1.61803398, breakurl 1.40, caption 56771 (revision), changepage
586 1.0c, courier 35058 (revision), csquotes 5.2k, datetime 2.60, dblfloatfix 1.0a, ec 1.0, enumitem 3.9, epstopdf 2.28,
587 eso-pic 3.0a, etoolbox 2.5k, fancyhdr 4.0, float 1.3d, fmtcount 3.07, fontaxes 1.0e, footmisc 5.5b, fp 2.1d, kastrup
588 15878 (revision), lastpage 1.2m, latexexpand 1.6, letltxmacro 1.6, lineno 4.41, listings 1.8d, logreq 1.0, microtype 2.8,
589 multirow 2.6, mweights 53520 (revision), newtx 1.640, pdfescape 1.15, pdftexcmds 0.33, pgf 3.1.8b, pgfplots 1.17,
590 preprint 2011, setspace 6.7a, soul 2.4, sttools 2.1, subfig 1.3, tex 3.14159265, texgyre 2.501, times 35058 (revision),
591 titlesec 2.13, trimspaces 1.1, txfonts 15878 (revision), ulem 53365 (revision), varwidth 0.92, wrapfig 3.6, xcolor
592 2.12, xkeyval 2.8 and xstring 1.83.

593

594 **FUNDING** No funding has been received for this project.

595 **DATA AVAILABILITY** As described above in §2.1, the source of curated SARS-CoV-2 infec-
596 tion count data used for the main analysis in this paper is the C19CCTF data, downloaded
597 using the script `download-wikipedia-SARS-CoV-2-charts.sh` and stored in the file
598 `Wikipedia_SARSCoV2_charts.dat` in the reproducibility package available at zenodo.4765705. The
599 data file is archived at zenodo.4765705/WP_C19CCTF_SARSCoV2.dat. The WHO data that was compared with
600 the C19CCTF data via a jump analysis (Fig. 1) was downloaded from [https://covid19.who.int/WHO-](https://covid19.who.int/WHO-COVID-19-global-data.csv)
601 `COVID-19-global-data.csv` and was archived on 6 May 2021.

602 **CODE AVAILABILITY** In addition to the SARS-CoV-2 infection count data for this paper, the full download-
603 ing of complementary data, calculations, production of figures, tables and values quoted in the text of the pdf
604 version of the paper are intended to be fully reproducible on any POSIX-compatible system using free-licensed
605 software, which, by definition, the user may modify, redistribute, and redistribute in modified form. The re-
606 producibility framework is technically a GIT branch of the MANEAGE package (Akhlaghi et al., 2021)⁵, earlier
607 used to produce reproducible papers (Infante-Sainz et al., 2020). The GIT repository commit ID of this version
608 of this paper is `subpoisson-72242ca`. The primary (live) GIT repository is [https://codeberg.org/boud/](https://codeberg.org/boud/subpoisson)
609 `subpoisson`, archived at `swh:1:rev:27ac91a5b79d4dfe6d17ee2a43d3b441efdb22c7`. The full reproducibility
610 package is archived at zenodo.4765705. Bug reports and discussion are welcome at [https://codeberg.org/](https://codeberg.org/boud/subpoisson/issues)
611 `boud/subpoisson/issues`.

612 **CONFLICT OF INTEREST** The author of this paper is aware of no financial or similar conflicts of interests.

613 **ORCID** *Boudewijn F. Roukema* ORCID: <https://orcid.org/0000-0002-3772-0250>

614 REFERENCES

- 615 AFN 2020, Nexta channel accuses the Ministry of Health of the Republic of Belarus of publishing censored data on
616 coronavirus (in Russian), *AFN*, <https://afn.by/news/i/275882>, Archived at Wayback
617 Abdi S., 2007, Bonferroni and Sidak corrections for multiple comparisons. Thousand Oaks, Sage, USA,
618 <https://personal.utdallas.edu/%7Eherve/Abdi-Bonferroni2007-pretty.pdf>,
619 Archived at Wayback
620 Afshordi N., Holder B., Bahrami M., Lichtblau D., 2020, Diverse local epidemics reveal the distinct effects of
621 population density, demographics, climate, depletion of susceptibles, and intervention in the first wave of COVID-
622 19 in the United States, *arXiv e-prints*, (arXiv:2007.00159)
623 Akaike H., 1974, A new look at the statistical model identification, *IEEE Trans. on Auto. Contr.*, 19, 716

⁵<https://maneage.org>

624 Akhlaghi M., Infante-Sainz R., Roukema B. F., Valls-Gabaud D., Baena-Gallé R., 2021, Towards Long-term and
625 Archivable Reproducibility, *Comp. in Sci. Eng.*, in press (arXiv:2006.03018)

626 Balashov V. S., Yan Y., Zhu X., 2020, Are Less Developed Countries More Likely to Manipulate Data During
627 Pandemics? Evidence from Newcomb-Benford Law, *arXiv e-prints*, (arXiv:2007.14841)

628 Barabási A.-L., 2005, The origin of bursts and heavy tails in human dynamics, *Nature*, 435, 207
629 (arXiv:cond-mat/0505371)

630 Behnel S., Bradshaw R., Citro C., Dalcin L., Seljebotn D. S., Smith K., 2011, Cython: The Best of Both Worlds,
631 *CiSE*, 13, 31

632 Billah A., Miah M., Khan N., 2020, Reproductive number of coronavirus: A systematic review and meta-analysis
633 based on global level evidence, *PLoS One*, 15, e0242128

634 Chowdhury R., et al., 2020, Dynamic interventions to control COVID-19 pandemic: a multivariate prediction mod-
635 elling study comparing 16 worldwide countries, *Eur. J. Epidemiol.*, 35, 389

636 Cole B., 2020, Russia accuses media of false coronavirus death numbers as Moscow officials say 60 percent of
637 fatalities not included, *Newsweek*, [https://www.newsweek.com/russia-accuses-media-false-](https://www.newsweek.com/russia-accuses-media-false-coronavirus-death-numbers-1503932)
638 [coronavirus-death-numbers-1503932](https://www.newsweek.com/russia-accuses-media-false-coronavirus-death-numbers-1503932), Archived at Archive Today

639 Croux C., Dehon C., 2010, Influence functions of the Spearman and Kendall correlation measures, *Stat. Methods*
640 *Appl.*, 19, 497

641 Endo A., Abbott S., Kucharski A. J., Funk S., 2020, Estimating the overdispersion in COVID-19 transmission using
642 outbreak sizes outside China, *Wellcome Open Res.*, 5, 67

643 Goh K.-I., Barabasi A.-L., 2006, Burstiness and Memory in Complex Systems, *Europhys. Lett. Assoc.*, 81, 4
644 (arXiv:physics/0610233)

645 He D., et al., 2020, Low dispersion in the infectiousness of COVID-19 cases implies difficulty in control, *BMC*
646 *Public Health*, 20, 1558

647 Huang L., Zhang X., Zhang X., Zhijian W., Zhang L., Xu J., et al. 2020a, Rapid asymptomatic transmission of
648 COVID-19 during the incubation period demonstrating strong infectivity in a cluster of youngsters aged 16–23
649 years outside Wuhan and characteristics of young patients with COVID-19: A prospective contact-tracing study,
650 *J. Infection*, 80, e1

651 Huang C., Wang Y., Li X., L. R., Zhao J., Hu Y., et al. 2020b, Clinical features of patients infected with 2019 novel
652 coronavirus in Wuhan, China, *Lancet*, 395, 97

653 Hunter J. D., 2007, Matplotlib: A 2d graphics environment, *CiSE*, 9, 90

654 Infante-Sainz R., Trujillo I., Román J., 2020, The Sloan Digital Sky Survey extended point spread functions, *MNRAS*,
655 491, 5317 (arXiv:1911.01430)

656 Jiang F., Zhao Z., Shao X., 2020, Time Series Analysis of COVID-19 Infection Curve: A Change-Point Perspective,
657 *arXiv e-prints*, (arXiv:2007.04553)

658 Johnson N., Kemp A. W., Kotz S., 2005, *Univariate Discrete Distributions* (3rd ed.). John Wiley & Sons, Inc., New
659 York, NY, USA, doi:10.1002/0471715816

660 Justel A., Peña D., Zamar R., 1997, A multivariate Kolmogorov-Smirnov test of goodness of fit, *Stat.Prob.Letters*,
661 35, 251

662 Keegan B. C., Tan C., 2020, A Quantitative Portrait of Wikipedia’s High-Tempo Collaborations during the 2020
663 Coronavirus Pandemic, *arXiv e-prints*, (arXiv:2006.08899)

664 Kendall M. G., 1938, A New Measure of Rank Correlation, *Biometrika*, 30, 81

665 Kendall M. G., 1970, *Rank Correlation Methods*, 4th edn. Griffin, London

666 Kim T., Lieberman B., Luta G., Pena E., 2020, Prediction Regions for Poisson and Over-Dispersed Poisson Regres-
667 sion Models with Applications to Forecasting Number of Deaths during the COVID-19 Pandemic, *arXiv e-prints*
668 , (arXiv:2007.02105)

669 Koch C., Okamura K., 2020, Benford’s Law and COVID-19 reporting, *Econ.Lett.*, 196, 109573

670 Kolmogorov A. N., 1933, Sulla Determinazione Empirica di Una Legge di Distribuzione, *Giornale dell’Istituto*
671 *Italiano degli Attuari*, 4, 83

672 Kramer A. E., 2020, “There Are No Viruses Here”: Leader of Belarus Scoffs at Lockdowns, *The New*
673 *York Times*, [https://www.nytimes.com/2020/04/25/world/europe/belarus-lukashenko-](https://www.nytimes.com/2020/04/25/world/europe/belarus-lukashenko-coronavirus.html)
674 [coronavirus.html](https://www.nytimes.com/2020/04/25/world/europe/belarus-lukashenko-coronavirus.html), Archived at Archive Today

675 Lauer S. A., et al., 2020, The Incubation Period of Coronavirus Disease 2019 (COVID-19) From Publicly Reported
676 Confirmed Cases: Estimation and Application, *Ann.Intern.Med.*, M20, 0504

677 Lee K.-B., Han S., Jeong Y., 2020, COVID-19, flattening the curve, and Benford’s law, *Physica A*, 559, 125090

678 Letowska E., Pacewicz P., 2020, Prof. Łętowska: To nie były wybory, ale plebiscyt. Uchybienia wyborcze rzucają
679 długi gęsty cień, *OKO.press*, [https://oko.press/prof-letowska-to-nie-byly-wybory-ale-](https://oko.press/prof-letowska-to-nie-byly-wybory-ale-plebiscyt)
680 [plebiscyt](https://oko.press/prof-letowska-to-nie-byly-wybory-ale-plebiscyt), Archived at Wayback

681 Li R., Pei S., Chen B., Song Y., Zhang T., Yang W., Shaman J., 2020, Substantial undocumented infection facilitates
682 the rapid dissemination of novel coronavirus (SARS-CoV-2), *Science*, 368, 489

683 Lloyd-Smith J. O., Schreiber S. J., Kopp P. E., Getz W. M., 2005, Superspreading and the effect of individual

684 variation on disease emergence, *Nature*, 438, 355
685 Marsaglia G., Tsang W. W., Wang J., 2003, Evaluating kolmogorov's distribution, *J.Stat.Soft.*, 8, 1
686 Mebane W. R. J., 2010, Fraud in the 2009 presidential election in iran?, *Chance*, 23, 6
687 Millman K. J., Aivazis M., 2011, Python for scientists and engineers, *CiSE*, 13, 9
688 Molina-Cuevas E. A., 2020, Choosing a growth curve to model the Covid-19 outbreak, *arXiv e-prints* ,
689 (arXiv:2007.03779)
690 Munck G. L., Verkuilen J., 2002, Conceptualizing and Measuring Democracy: Evaluating Alternative Indices, *Com-*
691 *parat.Polit.Stud.*, 35, 5
692 Newcomb S., 1881, Note on the Frequency of Use of the Different Digits in Natural Numbers, *American Journal of*
693 *Mathematics* , 4, 39
694 Nigrini M., Miller S. J., 2009, Data diagnostics using second order tests of Benford's Law,
695 *Auditing: J. Pract. & Theory*, 28, 305
696 Oliphant T. E., 2007, Python for scientific computing, *CiSE*, 9, 10
697 Papoulis A., Pillai U., 2002, Probability, Random Variables and Stochastic Processes, 4th edn. McGraw-Hill Europe
698 Poisson S.-D., 1837, Recherches sur la probabilité des jugements en matière criminelle et en matière civile ;
699 précédées des Règles générales du calcul des probabilités. Bachelier, Imprimeur-Libraire, Paris, [https://](https://gallica.bnf.fr/ark:/12148/bpt6k110193z/f218.image)
700 gallica.bnf.fr/ark:/12148/bpt6k110193z/f218.image
701 Porecha M., 2020, India records over 10,000 new Covid-19 cases for first time, *The Hindu* , [https://www.](https://www.thehindubusinessline.com/news/national/india-records-over-10000-new-covid-19-cases-for-first-time/article31810421.ece)
702 [thehindubusinessline.com/news/national/india-records-over-10000-new-covid-](https://www.thehindubusinessline.com/news/national/india-records-over-10000-new-covid-19-cases-for-first-time/article31810421.ece)
703 [19-cases-for-first-time/article31810421.ece](https://www.thehindubusinessline.com/news/national/india-records-over-10000-new-covid-19-cases-for-first-time/article31810421.ece), Archived at Archive Today
704 Reporters sans frontières 2021, Detailed methodology, , <https://rsf.org/en/detailed-methodology>,
705 Archived at Archive Today
706 Rouabah M. T., Tounsi A., Belaloui N. E., 2020, A mathematical epidemic model using genetic fitting algorithm
707 with cross-validation and application to early dynamics of COVID-19 in Algeria, *J.Fundam.Appl.Sci*, 12, 1253
708 (arXiv:2005.13516)
709 Roukema B. F., 2014, A first-digit anomaly in the 2009 iranian presidential election, *Journal of Applied Statistics*,
710 41, 164 (arXiv:0906.2789v6)
711 Roukema B. F., 2015, in Miller S. J., ed., , The Theory and Applications of Benford's Law. Princeton University
712 Press, Princeton, pp 223–232
713 Ruijter E., Détienne F., Baker M., Groff J., Meijer A. J., 2019, The Politics of Open Government Data: Understanding
714 Organizational Responses to Pressure for More Transparency, *Am.Rev.Publ.Admin.*, 50, 260
715 Schwarz G. E., 1978, Estimating the dimension of a model, *Ann.Statist.*, 6, 461
716 Sen P. K., 1968, Estimates of the regression coefficient based on Kendall's tau, *J. Amer. Stat. Assoc.*, 63, 1379
717 Shapiro S. S., Wilk M. B., 1965, An analysis of variance test for normality (complete samples), *Biometrika*, 52, 591
718 Smirnov N., 1948, Table for Estimating the Goodness of Fit of Empirical Distributions, *Ann. Math. Stat.* , 19, 279
719 Theil H., 1950, A rank-invariant method of linear and polynomial regression analysis, *Nederl. Akad. Wetensch.*,
720 *Proc.* , 53, 386
721 Thomas P., et al., 2017, If these data could talk, *Scientific Data*, 4, 170114
722 Wyrzykowski M., 2020, Former CT judge Prof. Wyrzykowski: The presidential elections in Poland will be held
723 under the pretence of legality, *Ruleoflaw.pl* , [https://ruleoflaw.pl/former-ct-judge-prof-](https://ruleoflaw.pl/former-ct-judge-prof-wyrzykowski-the-presidential-elections-in-poland-will-be-held-under-the-pretence-of-legality)
724 [wyrzykowski-the-presidential-elections-in-poland-will-be-held-under-the-](https://ruleoflaw.pl/former-ct-judge-prof-wyrzykowski-the-presidential-elections-in-poland-will-be-held-under-the-pretence-of-legality)
725 [pretence-of-legality](https://ruleoflaw.pl/former-ct-judge-prof-wyrzykowski-the-presidential-elections-in-poland-will-be-held-under-the-pretence-of-legality), Archived at Wayback
726 Yang L., Dai J., Zhao J., Wang Y., Deng P., Wang J., 2020, Estimation of incubation period and serial interval of
727 COVID-19: analysis of 178 cases and 131 transmission chains in Hubei province, China, *Epidemiol.Infect.*, 148,
728 e117
729 Yu H., Robinson D. G., 2012, The New Ambiguity of “Open Government”, *UCLA L. Rev. Disc.* , 59, 178
730 van der Walt S., Colbert S. C., Varoquaux G., 2011, The NumPy Array: A Structure for Efficient Numerical Com-
731 putation, *CiSE*, 13, 22 (arXiv:1102.1523)

732 A JHU CSSE DATA

733 The John Hopkins University Center for Systems Science and Engineering global time se-
734 ries data was downloaded on 6 May 2021 from [https://raw.githubusercontent.com/CSSEGISandData/COVID-19/master/csse_covid_19_data/](https://raw.githubusercontent.com/CSSEGISandData/COVID-19/master/csse_covid_19_data/csse_covid_19_time_series/time_series_covid19_confirmed_global.csv)
735 [csse_covid_19_time_series/time_series_covid19_confirmed_global.csv](https://raw.githubusercontent.com/CSSEGISandData/COVID-19/master/csse_covid_19_data/csse_covid_19_time_series/time_series_covid19_confirmed_global.csv),
736 from git commit 51CB3EE, and analysed using the same software and parameters as for the C19CCTF
737 data. Tables 7–10 show the equivalent of Tables 1–4, respectively. The rankings and ϕ_i estimates appear
738 mostly similar between the two datasets, with small differences. One difference is that the low ϕ_i^7 value
739 for India shown in Table 4 is absent in Table 10. In other words, while the media stated that the daily
740

Table 7. As in Table 1, for the JHU CSSE data: clustering parameters for the countries with the 10 lowest ϕ_i and 10 lowest ψ_i values, i.e., the least noise; extended version of table: zenodo.4765705/phi_N_full_jhu.dat.

country	ϕ_i' model					alternative analyses			
	N_i	P_i^{Poiss}	P_i^{KS}	ϕ_i	ψ_i	\hat{v}_i	ω_i	P_i^{KS}	ω_i
Syria	23121	0.48	0.94	0.72	0.004	0.94	0.72	0.48	0.00
Algeria	123272	0.04	0.19	0.98	0.002	0.20	1.00	0.04	0.00
Croatia	339412	0.27	0.89	3.24	0.005	0.89	3.24	0.70	1.02
Saudi Arabia	422316	0.00	0.83	3.67	0.005	0.66	3.55	0.62	2.43
New Zealand	2637	0.10	0.88	3.85	0.074	0.89	4.68	0.90	3.63
Albania	131419	0.00	0.16	4.90	0.013	0.17	4.90	0.09	3.76
Thailand	74921	0.29	0.99	5.37	0.019	0.99	5.37	0.96	3.80
Denmark	257182	0.00	0.97	5.56	0.010	0.99	5.56	0.91	5.50
Iceland	6498	0.33	1.00	5.96	0.073	0.99	5.96	0.95	4.27
Greece	352027	0.03	0.98	6.53	0.011	0.92	5.43	0.67	5.50
Algeria	123272	0.04	0.19	0.98	0.002	0.20	1.00	0.04	0.00
Russia	4792354	0.00	0.31	10.12	0.004	0.26	9.44	0.26	8.81
Syria	23121	0.48	0.94	0.72	0.004	0.94	0.72	0.48	0.00
Croatia	339412	0.27	0.89	3.24	0.005	0.89	3.24	0.70	1.02
Saudi Arabia	422316	0.00	0.83	3.67	0.005	0.66	3.55	0.62	2.43
Iran	2591609	0.00	0.33	11.61	0.007	0.17	10.00	0.25	9.66
Turkey	4955594	0.00	0.02	19.95	0.008	0.01	19.27	0.01	16.98
Denmark	257182	0.00	0.97	5.56	0.010	0.99	5.56	0.91	5.50
Hungary	785967	0.02	0.99	9.23	0.010	0.98	14.29	0.91	7.00
Belarus	363732	0.00	0.01	6.92	0.011	0.01	6.46	0.01	5.13

741 confirmed count in India first went above the 10,000-per-day psychological threshold on 12 June 2020
742 (Porecha, 2020), the JHU CSSE data crossed this threshold earlier, and contains noise that was unknown
743 at that time to the national Indian media and is absent from the C19CCTF data.

744 Another difference is that Saudi Arabia, Iran, and the United Arab Emirates have lowest-noise sub-
745 sequence dates detected in 2021 in the JHU CSSE Tables 8–10, while no country has lowest-noise
746 subsequences in 2021 in the C19CCTF data (Tables 2–4).

747 Table 12 shows that the JHU CSSE data generally find somewhat stronger anticorrelations between
748 the clustering parameters and PFI^{2020} compared to Table 6.

Table 8. As in Table 2, for the JHU CSSE data: least noisy 28-day sequences – clustering parameters for the countries with the 10 lowest ϕ_i^{28} values; extended table: zenodo.4765705/phi_N_28days_jhu.dat.

country	N_i	$\langle n_i^{28} \rangle$	P_i^{Poiss}	P_i^{KS}	ϕ_i^{28}	starting date
Algeria	123272	338.2	0.02	0.72	0.05	2020-08-18
Turkey	4955594	1014.5	0.03	1.00	0.14	2020-06-30
United Arab Emirates	529220	2884.9	0.01	0.07	0.15	2020-12-30
Belarus	363732	921.9	0.14	0.89	0.21	2020-05-08
Albania	131419	203.8	0.33	0.64	0.23	2020-09-27
Russia	4792354	5414.0	0.36	0.85	0.24	2020-07-19
Saudi Arabia	422316	332.5	0.54	0.78	0.43	2021-02-01
Syria	23121	70.0	0.19	0.91	0.50	2020-08-15
Iran	2591609	6594.5	0.14	0.41	1.51	2021-01-15
Georgia	315913	384.4	0.79	0.99	1.66	2020-09-17

Table 9. As in Table 3, for the JHU CSSE data: least noisy 14-day sequences – clustering parameters for the countries with the 10 lowest ϕ_i^{14} values; extended version of table: zenodo.4765705/phi_N_14days_jhu.dat.

country	N_i	$\langle n_i^{14} \rangle$	P_i^{Poiss}	P_i^{KS}	ϕ_i^{14}	starting date
United Arab Emirates	529220	3384.1	0.07	0.35	0.05	2021-01-11
Algeria	123272	336.4	0.06	0.80	0.05	2020-08-26
Turkey	4955594	971.6	0.12	0.86	0.11	2020-07-08
Belarus	363732	945.6	0.22	1.00	0.13	2020-05-12
Albania	131419	143.4	0.16	0.92	0.15	2020-09-01
Saudi Arabia	422316	337.7	0.32	0.79	0.20	2021-02-08
Russia	4792354	5165.5	0.47	0.51	0.28	2020-08-01
Syria	23121	76.6	0.42	0.96	0.35	2020-08-14
Poland	2811951	299.9	0.55	0.68	0.53	2020-06-17
Kenya	161393	126.2	0.54	0.91	0.57	2020-06-03

Table 10. As for Table 4, for the JHU CSSE data: least noisy 7-day sequences – clustering parameters for the countries with the 10 lowest ϕ_i^7 values; extended table: zenodo.4765705/phi_N_07days_jhu.dat.

country	N_i	$\langle n_i^7 \rangle$	P_i^{Poiss}	P_i^{KS}	ϕ_i^7	starting date
United Arab Emirates	529220	544.9	0.24	0.99	0.05	2020-04-27
Turkey	4955594	929.6	0.22	0.93	0.05	2020-07-15
Albania	131419	297.7	0.23	0.98	0.05	2020-10-18
Belarus	363732	947.9	0.60	0.94	0.05	2020-05-13
Algeria	123272	204.3	0.37	0.49	0.05	2020-10-14
Russia	4792354	5035.0	0.38	0.75	0.10	2020-08-09
Poland	2811951	297.0	0.51	0.99	0.10	2020-06-20
Saudi Arabia	422316	175.6	0.52	0.99	0.15	2021-01-13
Syria	23121	82.3	0.21	0.97	0.17	2020-08-14
Panama	365975	171.1	0.82	0.96	0.17	2020-05-09

Table 11. As for Table 5, Akaike (1974) and Bayesian (Schwarz, 1978) information criteria for the ϕ'_i and alternative analyses for the JHU CSSE data; plain-text version: zenodo.4765705/AIC.BIC_full_jhu.dat.

model	ϕ'_i		log. median		neg. binomial		2-day grouping		3-day grouping	
	AIC	BIC	AIC	BIC	AIC	BIC	AIC	BIC	AIC	BIC
	376.18	994.94	401.69	1020.44	498.00	1116.75	421.96	1032.94	239.83	811.89

Table 12. As for Table 6, Kendall τ statistic and its significance (two-sided) P^τ for the null hypothesis of no correlation between the ranking of PFI²⁰²⁰ and ϕ_i or ψ_i for the full data or subsequences, for the JHU CSSE data; plain-text version: zenodo.4765705/pfi_correlations_table.dat.

parameter	full		28-day		14-day		7-day	
	τ	P^τ	τ	P^τ	τ	P^τ	τ	P^τ
ϕ_i	-0.124	0.105	-0.158	0.0400	-0.175	0.0230	-0.232	0.00254
ψ_i	-0.165	0.0318	-0.162	0.0346	-0.163	0.0339	-0.194	0.0112